

THE EFFECT OF TEMPERATURE ON OIL/WATER RELATIVE PERMEABILITIES IN
MICROFLUIDIC MICROMODEL

by
Medet Madalimov

A thesis submitted to the Faculty and the Board of Trustees of the Colorado School of Mines in partial fulfillment of the requirements for the degree of Master of Science (Petroleum Engineering).

Golden, Colorado

Date _____

Signed: _____

Medet Madalimov

Signed: _____

Dr. Erdal Ozkan

Thesis Advisor

Golden, Colorado

Date _____

Signed: _____

Dr. Jennifer L. Miskimins

Professor and Head

Department of Petroleum Engineering

ABSTRACT

Over the last four decades, many studies have been conducted to investigate the effect of temperature on oil/water relative permeability. Many contradictions and disagreements have been observed in these studies. Some studies have shown the effect of temperature, others have disagreed with that by attributing changes to other experimental errors, such as viscous instabilities.

In this study, the effect of temperature on oil/water relative permeability was studied in a microfluidic micromodel system. First, the microfluidic micromodel fabrication procedures using Norland Optical Adhesive 81 (NOA81) was demonstrated. Images from two-phase flow displacement experiments were captured, processed and analyzed with MATLAB Image Processing Toolbox. The Jones and Roszelle method and an alternate approach based on Darcy's law were used to calculate oil/water relative permeabilities from displacement experiments.

The results of this study indicated that, as temperature went up, oil relative permeability increased, and residual oil saturation decreased. There were some disagreements in water relative permeability data obtained by Darcy's law and the Jones and Roszelle method. This thesis explains the experimental setup and procedure, measurement and calculation techniques, and assumptions made, documents the data and results, provides a discussion of the conclusions and recommendations for future work.

TABLE OF CONTENTS

| | |
|--|------|
| ABSTRACT..... | iii |
| LIST OF FIGURES | iv |
| LIST OF TABLES | viii |
| ACKNOWLEDGEMENTS | ix |
| CHAPTER 1 INTRODUCTION | 1 |
| 1.1. Problem Statement..... | 1 |
| 1.2. Objectives | 2 |
| 1.3. Methods of study | 2 |
| 1.3.1. Johnson – Bossler – Naumann method..... | 3 |
| 1.3.2. Darcy Equation method | 6 |
| 1.4. Literature review | 7 |
| 1.5. Micromodel | 11 |
| 1.6. Organization of the Thesis | 15 |
| CHAPTER 2 METHODOLOGY | 16 |
| 2.1. Micromodel pattern | 16 |
| 2.2. Fabrication of NOA81 micromodel | 16 |
| 2.3. Experimental preparation and set-up | 19 |
| 2.4. Fluid and NOA81 properties | 21 |
| 2.5. Data analysis | 25 |
| 2.5.1. Micromodel absolute permeability | 25 |
| 2.5.2. Data processing from images | 27 |
| 2.5.3. Relative permeability | 31 |

| | |
|---|----|
| CHAPTER 3 EXPERIMENTAL RESULTS AND ANALYSIS | 36 |
| 3.1. Relative permeability using Darcy Equation method | 36 |
| 3.2. Relative permeability using Jones and Roszelle method | 41 |
| 3.3. Effect of temperature on oil/water relative permeability | 44 |
| CHAPTER 4 CONCLUSION AND DISCUSSION | 51 |
| LIST OF SYMBOLS | 53 |
| REFERENCES | 55 |
| APPENDIX A | 59 |
| APPENDIX B | 61 |

LIST OF FIGURES

| | |
|--|----|
| Figure 1.1: Estimated relative permeability – saturation curves for different capillary numbers (Tsakiroglou et al. 2003)..... | 13 |
| Figure 2.1: Original (a) and CAD format (b) of rock cross-section pattern. Red rectangular area was chosen for the micromodel network design. | 17 |
| Figure 2.2: Network design with 1130 μm x 850 μm dimension. Dashed area indicates solid material. | 18 |
| Figure 2.3: NOA81 micromodel fabrication process. NOA81 to NOA81 half-curing bonding method..... | 19 |
| Figure 2.4: Schematic of experimental set-up for displacement test with ROC..... | 20 |
| Figure 2.5: Experimental Set-up of displacement experiment with ROC | 21 |
| Figure 2.6: Mineral oil viscosity vs temperature | 22 |
| Figure 2.7: Water viscosity vs temperature | 22 |
| Figure 2.8: Pendant drop of water at 20°C, 50° and 70°C..... | 23 |
| Figure 2.9: Oil – Water Interfacial Tension versus Temperature | 23 |
| Figure 2.10: Fully water saturated micromodel, $S_w = 100\%$ | 26 |
| Figure 2.11: Sequence of captured images from oil-water displacement test with Photo Director8 | 27 |
| Figure 2.12: Preprocessed sequence of images from oil – water displacement test with ImageJ | 28 |
| Figure 2.13: Water saturation determination from binary images (a) at fully water saturated, (b) water saturation = 73.27% and (c) at 50.41% water saturation..... | 29 |
| Figure 2.14: Image sequence of water-oil displacement test..... | 30 |
| Figure 2.15: Water saturation vs Cumulative Water Injection in PV unit..... | 30 |
| Figure 3.1: Image consequences from an oil – water displacement test conducted at 50°C | 36 |
| Figure 3.2: Saturation vs time in oil-water displacement test..... | 37 |
| Figure 3.3: Saturation vs Cumulative PV Injection of Oil..... | 37 |

| | |
|---|----|
| Figure 3.4: Water relative permeability using the DE method | 38 |
| Figure 3.5: Image sequence from water – oil displacement test at 50°C..... | 39 |
| Figure 3.6: Water saturation profile versus time in water – oil displacement test at 50°C | 40 |
| Figure 3.7: Water saturation versus Cumulative injected water in pore volume..... | 40 |
| Figure 3.8: Oil relative permeability using the DE method..... | 41 |
| Figure 3.9: Cumulative injected water and produced oil versus time in water – oil displacement experiment | 43 |
| Figure 3.10: Relative permeability based on the Jones and Roszelle method | 43 |
| Figure 3.11: Oil and water relative permeabilities at ambient temperature using the DE method..... | 45 |
| Figure 3.12: Oil and water relative permeability at ambient temperature using the Jones and Roszelle method..... | 46 |
| Figure 3.13: Oil and water relative permeabilities at 50° temperature using the DE method | 47 |
| Figure 3.14: Oil and water relative permeability curves at 50° using Jones and Roszelle method..... | 47 |
| Figure 3.15: Oil and water relative permeabilities at 70° using the DE method | 48 |
| Figure 3.16: Oil and water relative permeabilities at 70°C using the Jones and Roszelle method..... | 49 |
| Figure 3.17: Residual oil saturation | 49 |
| Figure 3.18. Error bars of residual oil saturation change with temperature | 50 |
| Figure 3.19: Temperature effect on Water – oil permeability curves..... | 50 |

LIST OF TABLES

| | |
|---|----|
| Table 1.1: A summary of the recent experimental studies of temperature effects on relative permeability | 10 |
| Table 2.1: Oil and water capillary number at different temperatures | 24 |
| Table 2.2: Absolute permeability measurements | 26 |
| Table 3.1: Relative water permeability calculation the DE method | 38 |
| Table 3.2: Relative oil permeability calculation by the DE method | 41 |
| Table 3.3: Oil and water relative permeabilities using the Jones and Roszelle method | 42 |

ACKNOWLEDGEMENTS

I would like to express my sincere gratitude to Dr. Erdal Ozkan, my graduate advisor for providing me full support and guidance since I started my graduate program at Colorado School of Mines. I also would like to thank to my committee members Dr. Xiaolong Yin and Dr. Luis Zerpa for their help, valuable comments and guidance.

I am grateful for Denise Winn-Bower and Joe Chen for helping me with administrative and laboratory tasks during my study at CSM. Special thanks to Shaken Kenzhekhanov for his help to fulfill my work.

I would like to thank Bolashak for financial support.

Finally, and most importantly, I want to give special thanks to my family and wife, Saltanat Kassymgaliyeva, for her support and motivation to accomplish this work.

CHAPTER 1

INTRODUCTION

This thesis presents the research performed under the Unconventional Reservoir Engineering Project (UREP) for the partial fulfillment of the requirements for a Master of Science (MSc) degree in Petroleum Engineering Department at the Colorado School of Mines. The work investigated the effect of temperature on oil and water relative permeabilities by displacement tests conducted through microfluidic micromodels. Micromodels have been popular lately to visualize and measure multiphase flows through porous media. Most of the applications of micromodels in studies of flow and transport in porous media are related to the immiscible displacement of two fluid phases. The most commonly used unsteady – state techniques to calculate relative permeability are Johnson – Bossler – Naumann (Johnson et al. 1957) and Darcy Equation (DE) methods. This thesis presents the workflow of image processing of displacement tests and the relative permeabilities calculated with the Jones and Roszelle method, which is an extension of the Johnson et al. technique, and the Darcy Equation method. The results obtained at different temperatures and the observed limits are documented in the conclusion section.

1.1. Problem Statement

Knowledge of the physical rock properties is of crucial importance for understanding the nature of a reservoir. Permeability characterizes the ability of the rock to let fluid flow through the porous media. When only one fluid is presented in the porous media system, this transport coefficient is called absolute permeability. Otherwise, we must take reference to the effective permeabilities of each of the immiscible fluids in the porous media system. The ratio of the effective to the absolute permeability is the relative permeability.

In a two-phase flow system, wetting and non-wetting phases flow together in a porous medium and each of them follows its own distinct paths. When two immiscible fluids flow simultaneously, they interfere, and the sum of their effective permeabilities is less than the absolute permeability. In other words, the sum of relative permeabilities is less than one. In two-phase flow displacement process in micromodel we assume that a certain number of pores and throats are available for wetting phase to flow, while the remainder is accessible by the non-wetting phase.

For modeling the thermal oil recovery process, one needs to know not only the relative permeability at the original reservoir temperature but also the effect of temperature on relative permeability. A number of studies have considered the effect of temperature on oil/water relative permeability recently with no solid conclusion; several researchers have concluded that temperature had a considerable effect on two-phase relative permeability, while others have reported no significant influence of temperature (Akin et al. 1999).

1.2. Objectives

The problem stated above provides motivation for this study and defines the following objectives:

1. Estimate oil and water relative permeabilities from microfluidic micromodels.
2. Study the temperature effect on oil and water relative permeabilities.
3. Develop efficient approach to fabricate microfluidic micromodels.

1.3. Methods of Study

Laboratory measurement methods for obtaining the two-phase relative permeability data based on flow experiments have been described in the literature (Johnson et al. 1957). Two

different techniques, steady state (SS) and unsteady state (USS), can be conducted to determine relative permeability. In this study, we use the USS technique.

The USS technique is based on the analysis of data obtained from an immiscible displacement process. For a two-phase system, the porous media (microfluidic micromodel in our case) is flooded with the displacing phase (water). The first step is the determination of the effective permeability to oil at irreducible water saturation, $k_{eo}@S_{wi}$. Then, the injection of water at constant pressure is initiated; the displacement process is recorded. Consequently, water saturation in the system increases over time above the irreducible saturation, S_{wi} , and additional oil and water are produced, eventually leading to a plateau of cumulative oil production versus time. At some point, oil production will stop and only water will come out of the core. The injection of water is continued further to the residual oil saturation, S_{or} , enabling calculation of the effective permeability of water, $k_{ew}@S_{or}$.

The two methods to determine relative permeability from USS tests, JBN and DE methods, are discussed below.

1.3.1. Johnson – Bossler – Naumann (JBN) method.

Buckley and Leverett (Buckley and Leverett 1941) developed the equations governing the displacement of one fluid by another in a porous medium. Later, Welge (1951) presented a method to calculate the saturation and the ratio of relative permeabilities of the displacing phase and the displaced phase based on the Buckley – Leverett theory. JBN method (Johnson et al. 1957) is based on Welge's solution of the flow equation to calculate the phase relative permeabilities from displacement data. The JBN method calculates relative permeabilities as a function of effluent (outlet) fluid saturation.

Before describing the JBN method, the fractional flow equation that relates the ratio of relative permeabilities to the experimental data, which are measured in a typical displacement test must be derived (see full derivation process in Appendix A). Equation 1.1 or 1.2 is the fractional flow equation for the displacement of oil by water for a horizontal displacement and neglecting the capillary pressure gradient.

$$f_w = \frac{1}{1 + \left[\frac{k_{ro}\mu_w}{k_{rw}\mu_o} \right]} \quad (1.1)$$

$$f_w = \frac{1}{1 + \left[\frac{k_{ro}\mu_w}{k_{rw}\mu_o} \right]} \quad (1.2)$$

The JBN method (Johnson et al. 1957) is probably the most popular technique to determine relative permeability relationship for each flowing phase in petroleum engineering. The data required for the JBN method are the pore volumes of the injected and produced fluids, pressure drop across the system, and fluid property data such as viscosity.

Johnson et al. adopted the approach proposed by Welge (1951) to determine the average and outlet water saturation (considering water as the displacing phase) by Equations 1.3 and 1.4:

$$S_{w2} = \overline{S_w} - Q_{wi} \frac{d\overline{S_w}}{dQ_{wi}} \quad (1.3)$$

$$\overline{S_w} = S_{wi} + \frac{\text{cumulative volume of oil produced}}{\text{pore volume of the sample}} \quad (1.4)$$

The main contribution of Johnson et al. (1957) was the method they proposed to determine the individual-phase relative permeabilities. The procedure begins with the integration of the pressure gradient across the core sample:

$$\Delta p = - \int_0^L \frac{\partial p}{\partial x} dx \quad (1.5)$$

The pressure gradient might be represented by Darcy's law:

$$\frac{\partial p}{\partial x} = - \frac{\mu_o u f_o}{k k_{ro}} \quad (1.6)$$

Using the Buckley – Leverett theory:

$$dx = dx_{sw} = L Q_{wi} df'_w = L \frac{df'_w}{f'_w} \quad (1.7)$$

$$\Delta p = - \frac{\mu_o u L}{k f'_w} \int_0^{f'_w} \frac{f_o}{k_{ro}} df'_w \quad (1.8)$$

$$\int_0^{f'_w} \frac{f_o}{k_{ro}} df'_w = - \frac{k f'_w \Delta p}{\mu_o u L} \quad (1.9)$$

When the system is at its initial saturation condition (before oil displacement by water starts), using Darcy's law we can write:

$$\left(\frac{u}{\Delta p} \right)_i = - \frac{k k_{ro, max}}{\mu_o L} \quad (1.10)$$

$$\int_0^{f'_w} \frac{f_o}{k_{ro}} df'_w = \frac{f'_w}{k_{ro, max}} \frac{\left(\frac{u}{\Delta p} \right)_i}{\left(\frac{u}{\Delta p} \right)} \quad (1.11)$$

Also, a new quantity called relative injectivity, I_r , is defined in terms of the intake capacity $(u/\Delta P)$ by Equation 1.12:

$$I_r = \frac{\left(\frac{u}{\Delta P} \right)}{\left(\frac{u}{\Delta P} \right)_i} \quad (1.12)$$

In Equation 1.12, $(u/\Delta P)$ is the intake capacity at any given displacement or flood stage, whereas $(u/\Delta P)_i$ represents intake capacity at the beginning of the flood.

By differentiating Eq 1.11 with respect to f'_w and combining with I_r , we obtain the following:

$$\frac{f_o}{k_{ro}} = \frac{d(f'_w/I_r)}{d(f'_w)} \quad (1.13)$$

Combining Equations 1.14 and 1.13 yields the practical equation to find the relative permeability to oil:

$$k_{ro} = f_o \frac{d[1/Q_{wi}]}{d[1/Q_{wi}I_r]} \quad (1.14)$$

The water relative permeability is then given by:

$$k_{rw} = k_{ro} \frac{\mu_w(1-f_o)}{\mu_o f_o} \quad (1.15)$$

In this study, an extended form of JBN method to measure relative permeability proposed by Jones and Roszelle (Jones and Roszelle 1978) was used, which also combines the Welge analysis and the differentiation of pressure drop and flow rate information to obtain relative permeabilities. The detailed workflow to obtain relative permeability using the Jones and Roszelle method is explained in Chapter 2.

1.3.2. Darcy Equation (DE) Method

The DE method based on Darcy's law yields the oil and water relative permeabilities as a function of the average water saturation as follow:

$$k_{eo} = \frac{q_o \mu_o L}{A \Delta p} \text{ at } S_w \quad (1.16)$$

$$k_{ew} = \frac{q_w \mu_w L}{A \Delta p} \text{ at } S_w \quad (1.17)$$

where Δp , is the pressure drop when the average water saturation is determined. q_o and q_w represent the volumetric flow rates of oil and water respectively. The relative permeabilities of oil and water are determined, by dividing the calculated effective permeabilities by the absolute permeability.

1.4. Literature Review

Several experimental studies have been published in the literature over the past four decades with contradictory results regarding the effect of temperature on two-phase relative permeabilities as well as the residual oil saturation in porous media (Akin et al. 1999). In addition to the disagreement on the generality of such effects, these studies did not agree on the possible mechanism causing these effects. Therefore, this study aims to determine the effect of temperature on oil-water relative permeability curves using Darcy's equation in a microfluidic system. Additionally, we examine the use of unsteady-state relative permeability estimation method and compare it to Darcy's method.

Edmondson (1965) investigated the effects of temperature on Berea cores using refined oils and an unsteady state experimental technique. He reported a reduction in residual oil saturation and the observation that the relative permeability ratio of oil to water shifted toward a higher water saturation as the temperature increased.

Poston et al. (1970) observed an increase in irreducible water saturation and a decrease in residual oil saturation with increasing temperature on an unconsolidated sand sample using refined oils. Furthermore, they found that relative permeabilities to both water and oil increased with higher temperatures.

Clossmann et al. (1985) concluded that tar and water relative permeability curves moved towards lower water saturation on frozen Peace River cores using the steady-state technique. Maini and Batcky (1985) found an increase in irreducible water saturation and a decrease in residual oil saturation as the temperature went up. Moreover, relative permeability to oil decreased while relative permeability to brine remained unchanged with increasing temperature.

Polikar et al. (1986) studied the effect of temperature on relative permeability conducting steady-state and unsteady-state relative permeability experiments using Athabasca bitumen and deionized water. The JBN technique was used to analyze their results. They concluded that there was no significant temperature effect on residual oil and irreducible water saturation, as well as on the relative permeability of either phase. Moreover, they observed that the steady- and unsteady-state techniques resulted in similar relative permeability curves.

Maini and Okazawa (1987) used the unsteady-state technique on unconsolidated silica sand using Bodo stock tank oil and de-ionized water. They found an increase in relative permeability to water with increasing temperature. Also, they obtained the most reliable data at residual oil saturation after three pore volumes injected.

Watson and Ertekin (1988) investigated the temperature gradient effect on oil–water relative permeability using the steady-state displacement technique. They concluded that changing temperature gradient caused a decrease in irreducible water and residual oil saturation. Furthermore, they found that the relative permeabilities to both oil and water decreased with increasing temperature.

Contradicting previous researchers, Polikar et al. (1990) reported no significant effect of temperature on relative permeability and saturation data up to 200°C. They used the steady-state

technique to measure the relative permeability of Athabasca bitumen using unconsolidated Ottawa sand as the porous medium.

Similar conclusions were reached by Muqeem et al. (1995), who conducted steady-state two- and three-phase relative permeability experiments at 75°C and 125°C using unconsolidated silica sand with refined oil, brine and nitrogen gas.

Kumar and Inouye (1994) conducted unsteady-state experiments at different temperatures and analyzed the result using the JBN technique. From their observations, the relative permeability data obtained at ambient conditions could be used for high temperatures if the wettability and viscous ratio was similar.

Akhlaghinia et al. (2013) measured heavy oil–water relative permeabilities at 28°C, 40°C and 52°C temperatures. They observed that the oil relative permeability first increased (from 28°C to 40°) and then decreased.

Zhang et al. (2017) investigated the effect of temperature on the oil–water relative permeability for sandstone reservoir. They concluded that irreducible water saturation increases linearly and residual oil saturation nonlinearly with increasing temperature. Oil and water relative permeabilities increase under the same water saturation and crossover saturation moves to the right in the relative permeability–saturation curve.

Qin et al. (2018) used a heavy–oil sample to investigate the effects of temperature on relative permeabilities. They observed that water saturation linearly increases, and residual oil saturation nonlinearly decreases with increasing temperature. Both oil and water relative permeabilities increase with temperature.

Table 1.1: A summary of the recent experimental studies of temperature effects on relative permeability

| Ref | Technique | Fluids | Temperature range | End-Point Saturation | Relative Permeability |
|---------------------------|------------------------|-----------------------------------|-------------------|--|---|
| Edmondson (1965) | Unsteady State (Welge) | Refined Oils | Room – 260°C | $S_{or} \downarrow T \uparrow$ | shifted |
| Clossmann et al. (1985) | Steady State | Altered-unaltered-deasphalted tar | 196°C | not presented | k_{rw} shifted to lower S_w |
| Maini and Batcky (1985) | Unsteady State | Stock Tank Oil | room-272°C | $S_{wirr} \uparrow T \uparrow$ $S_{or} \downarrow T \uparrow$ | $k_{ro} \downarrow T \uparrow$ $k_{rw} \rightarrow T \uparrow$ |
| Polikar et al. (1986) | Steady State | Refined Oil (Soltrol 170) | room-150°C | $S_{wirr} \uparrow T \uparrow$ | $k_{ro}, k_{rw} \downarrow T \uparrow$ |
| Maini and Okazawa (1987) | Unsteady State | Bodo Stock Tank Oil+3.5% ether | room-200°C | not presented | $k_{rw} \uparrow T \uparrow$ $k_{ro} \downarrow \uparrow T \uparrow$ |
| Watson and Ertekin (1988) | Unsteady State | Oil and water | | $S_{wirr} \downarrow T \uparrow$ $S_{or} \downarrow T \uparrow$ | $k_{rw} \downarrow T \uparrow$ $k_{ro} \downarrow T \uparrow$ |
| Polikar et al. (1990) | Steady State | Athabasca Bitumen | room-200°C | independent | independent |
| Muqem et al. (1995) | Steady State | Refined Oil+N2 | 75°C & 125°C | not presented | not presented |
| Kumar and Inouye (1994) | Unsteady State | SJV Oil-GulfLight + SJV | room-150°C | independent | Shifted |
| Akhlaghinia et al. (2013) | Unsteady State | | 28 – 52°C | not presented | $k_{ro} \uparrow \downarrow$ |
| Zhang et al. (2017) | Unsteady State | Oil | Up to 100°C | $S_{wr} \uparrow T \uparrow$ $S_{or} \downarrow T \uparrow$ | $k_{rw} \uparrow T \uparrow$ $k_{ro} \uparrow T \uparrow$ |
| Qin et al. (2018) | USS | Heavy oil | Up to 200 °C | $S_{wr} \uparrow T \uparrow$ $S_{or} \downarrow T \uparrow$ | $k_{rw} \uparrow T \uparrow$ $k_{ro} \uparrow T \uparrow$ |

Table 1.1 summarized the results obtained from the studies mentioned above. The observations show that there is no conclusive agreement on the effect of temperature on oil/water relative permeabilities. Some studies noted above showed an effect of temperature, while others disagreeing with that conclusion and address the changes to viscous instabilities and to other experimental errors. One of the reasons for experimental divergence from previous studies might be errors in saturation measurements (Akin et al. 1999). To overcome this problem, conducting a displacement experiment in microfluidic micromodels has been suggested and used in this study.

In this study, saturation was determined from a displacement experiment using the image processing technique and two methods of relative permeability measurements were used. First, the DE method is used to obtain relative permeability of displaced fluid by calculating volumetric displacement rate. Next, the Jones and Roszelle method is used to determine oil/water relative permeabilities. The accuracy of DE and Jones and Roszelle techniques in oil/water relative permeabilities estimation and its implication on the interpretation of the effect of temperature on relative permeabilities are discussed in Part 4. Also, experimental results and analysis are presented.

1.5. Micromodel

The oil and gas reservoir engineering presents tremendous opportunities for microfluidics, both for informing their subsurface operations and for fluid property analysis. Microfluidics is known as the science and technology of systems that process or manipulate small amounts (10^{-9} to 10^{-18} liters) of fluids using channels with dimensions of tens to hundreds of micrometers. They are also called “Lab on a Chip” because many experiments, which are conventionally conducted in a lab, can now be done on a small chip. Microfluidic networks can usually offer an unprecedented

pore-scale resolution of the critical transport phenomena. Microfluidic chips with flow geometries resembling those in porous media – have long been applied in this field. They are standardized tools to visualize and measure multiphase flow through porous media.

Most of the applications on lab on a chip studies of flow in porous media are related to the immiscible displacement of two–fluid phases. Processes of oil displacing water and water displacing oil, also, the mechanisms that dominate them, like viscous and capillary fingering, have been studied with microfluidic micromodels (Zhang et al. 2011; Ferer et al. 2004; Grate et al. 2010).

One of the first attempts to study two–phase flow and the relevant displacement mechanisms was conducted by Lenormand et al. (1983). They used a transparent polyester resin microfluidic micromodel with channels in the form of a network of capillary ducts. They found the displacement of the meniscus formed by the two–phases under different conditions like piston–type motion and snap–off. Wu et al. (2014) studied the effect of two-phase gas slip effect in nanofluidic chip. In that work, a lab on a chip approach was developed to visualize directly two-phase flow behavior in nanochannels with an advanced epifluorescence microscopy method combined with a nanofluidic chip. Xu et al. (2014) investigated the effect of pore geometry and interfacial tension on constant-pressure-gradient water–oil displacement efficiency using oil–wet polydimethylsiloxane microfluidic porous media analogs. An important application of microfluidic micromodels has been in the measurement of two – phase flow properties that cannot be determined with standard experiments, like phase saturation. Tsakiroglou et al. (2003) used micromodels to study the influence of the capillary number on non – equilibrium immiscible displacement in two–phase flow experiments. They showed that relative permeabilities of the two phases are not only a function of saturation but also depend on capillary numbers (Figure 1.1).

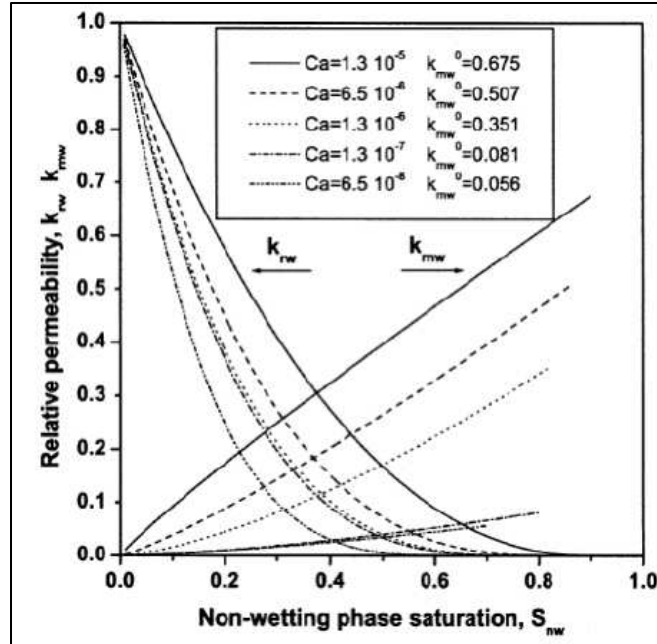


Figure 1.1.: Estimated relative permeability – saturation curves for different capillary numbers (Tsakiroglou et al. 2003).

Tsakiroglou et al. performed their measurement with a glass-etched micro-model, initially filled with the wetting phase (distilled water with methylene blue). The non-wetting phase (paraffin oil) was then injected into the network, at a fixed flow rate by a syringe pump. With the use of a CCD camera, successive shots of the displacement were captured from a central region of the network. The pressure drop along this central region of the network was measured with a differential pressure transducer with respect to time. This procedure allowed the determination of saturation and relative permeability of each phase as a function of time. Alternatively, Chang et al. (2009) calculated relative permeability by keeping a constant pressure head difference between the wetting and the non-wetting phases. For drainage, the non-wetting phase was introduced into a micro-model that was already fully saturated with the wetting phase, while the wetting phase flow rate was measured. This was continued until steady-state was reached. Images from the micro-model were taken with the use of a CCD camera. The main issue in such measurements is the determination of accurate phase pressures and phase saturations. While the latter depends on

the resolution of the visualization set up and can be usually quantified, the former is very difficult to measure. Especially, in a complex geometry with very small dimensions, it is practically impossible to measure local pressure within the micromodel (Karadimitriou 2013).

Soft lithography technique, which refers to methods for making structures using “soft” materials like photomasks, is one of the most popular methods to fabricate micromodels (Quake and Scherer 2000; Rogers and Nusso 2005; Wang et al. 2005). It is mostly preferred to fabricate very small, simple geometric structures on the micro- and nano-scale.

In this study, the experiments were conducted in microfluidic devices made by NOA81 with pore throat dimensions of 10-15 μm . NOA81 products generally have the following components: 1,1,1-tris (mercaptomethyl)-propane, trimethylpropane diallyl ether and isophorane diisocyanate. Under UV light, thiolene and thiourethane bonds form and, thus, the material is cured (Kenzhekhanov 2016).

NOA81 has the following properties to work as a microfluidic device material (Kenzhekhanov 2016):

1. Cured NOA81 has a light-yellow color but is perfectly transparent.
2. Compared to PDMS, NOA81 has better chemical resistance to organic solvents. Also, NOA81 is impermeable to both air and water vapor (Kenzhekhanov 2016).
3. Many surface treatments of NOA81 are available to simulate common wettability conditions of porous media. Previous researchers (Silvestrini et al. 2012, Wagli et al. 2011) have provided methods to change NOA to either hydrophilic or hydrophobic for specific use.

4. NOA81 has higher Young's modulus (around 1GPa) than PDMS (around 2.5 MPa) and bonding of NOA is stronger than PDMS (Kenzhekhanov 2016).

5. Fabrication of NOA81 devices is simple and fast.

1.6. Organization of the Thesis

This thesis is divided into four chapters, namely: introduction, methodology, experimental results and analysis, conclusion and discussion.

Chapter 1 contains the background of this study, problem statement, methods to calculate relative permeability from displacement experiment and outline of this thesis. Also, it presents recent studies of the effect of temperature on relative permeability and applications of micromodels in studies of flow and transport in porous media.

Chapter 2 discusses the methodology of the research. It explains the microfluidic micromodel fabrication workflow as well as the porous media's network design. Fluid properties, experimental set-up and preparation are presented. Data analysis shows the workflow of preprocessing the data obtained from experiments. Captured images and tests measurement are analyzed to obtain saturation and relative permeability.

Chapter 3 shows the experimental results and the analysis of data. Data obtained from different experiments compiled to identify the effect of temperature on two-phase displacement tests.

Finally, Chapter 4 presents the conclusions and discussion of the results. Recommendations for further research is also presented.

The codes for image processing are provided in the Appendix.

CHAPTER 2

METHODOLOGY

In this chapter, we present microfluidic micromodel fabrication process and network pattern. Also, fluid properties and experimental set-up and preparation are presented. Data analysis section presents absolute permeability and relative permeability calculations. In the end, we illustrate the preprocessing and analysis of captured images from two-phase displacement tests.

2.1. Micromodel pattern

In this study, scanned images of a rock cross-section, obtained from KAIA Corp. was used for network design. The sample description by KAIA Corp. indicated upper very fine- to lower coarse-grained, subrounded to rounded, moderately to moderately well sorted, quartzose sandstone; lithic fragments, altered grains, and heavy minerals were also present. Figure 2.1 illustrates the cross-section pattern. Figure 2.2 shows the micromodel pattern with a dimension of $1130\ \mu\text{m} \times 850\ \mu\text{m}$. The depth of the channels is $15\ \mu\text{m}$. The diameter of the inlet and outlet channels are $100\ \mu\text{m}$. Porosity of the network is 26%, which reflects the average value for high permeability sandstone formations.

2.2. Fabrication of NOA81 micromodel

Our approach of micromodel device fabrication is based on the techniques of soft lithography, specifically rapid prototyping and replica molding. Rapid prototyping starts from creating a network media design in a computer-aided design (CAD) program. A high-resolution image setter then prints this network on transparency, which serves as photomask in contact photolithography to produce a positive relief of photoresist on silicon wafer. The etching procedure

is standard, and the details may be found in Lin (2009). We refer to this positive relief as “master”, which is used for the casting of NOA81 devices. Two-layer etching is applied to make porous medium channels, which are 15- μm deep, and the inlet and outlet channels, which are 100- μm deep.

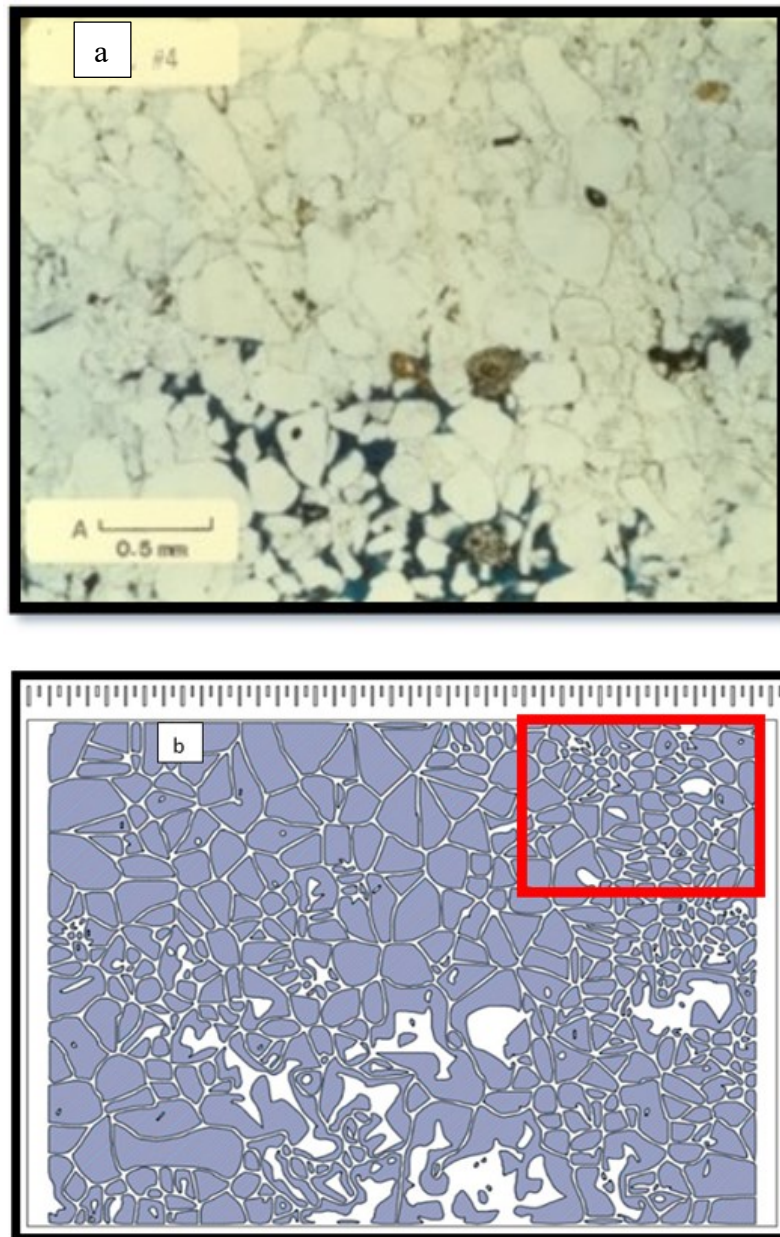


Figure 2.1: Original (a) and CAD format (b) of rock cross-section pattern. Red rectangular area was chosen for the micromodel network design.

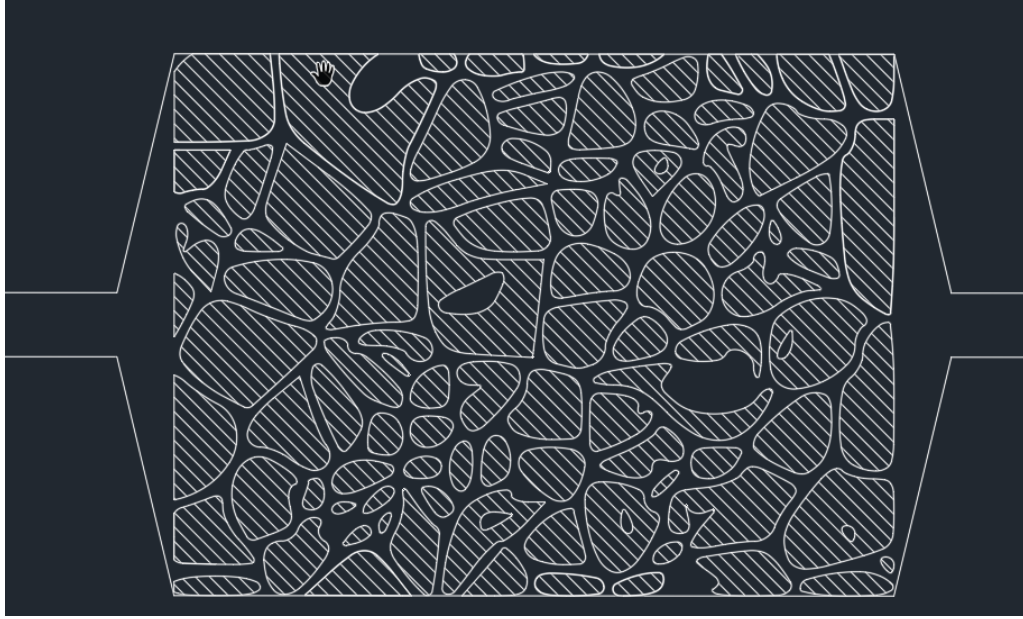


Figure 2.2: Network design with 1130 μm x 850 μm dimension. Dashed area indicates solid material.

Poly (dimethylsiloxane) polymer (PDMS) was used as an intermediate mold to transfer an etched pattern from the silicon wafer to NOA81. PDMS preparation was accomplished by using the Sylgard 184 Silicone Elastomer Kit. The elastomer and curing agent were mixed at a 10:1 ratio. Then, PDMS master was molded from the silicon wafer and developed in oven for 8 hours at 60°C. After the development, PDMS master was peeled off from the silicon wafer.

Based on the bonding recommendation of Kenzhekhanov (2016), we decided to use half-curing method (Levachee et al. 2012). This approach demonstrates strong NOA81-to-NOA81 bonding in crude oil environment. In the half-curing method, the network design is transferred from PDMS master to NOA81 by UV-light exposure (Figure 2.3, steps 1-2). Similar approach was used to prepare glass slide with NOA81 substrate on top (Figure 2.3, step 3-4).

The flat NOA81 substrate was cured by UV light only for 40 sec that left its surface sticky for further bonding. Then, the patterned NOA81 substrate was pressed against flat NOA81

substrate (Figure 2.3, step 5). Afterwards, UV-light exposure for 60 sec secured the bonding strength (Figure 2.3, step 6). A UVGL -56 (Entela) 365 nm long-wave UV lamp was used to cure NOA81. Then, tubing (ID = 0.51mm, OD= 1.52 mm) was connected to the micromodel and sealed with epoxy glue (Figure 2.3, step 7). Figure 2.3, step 8 shows the example of the final micromodel.

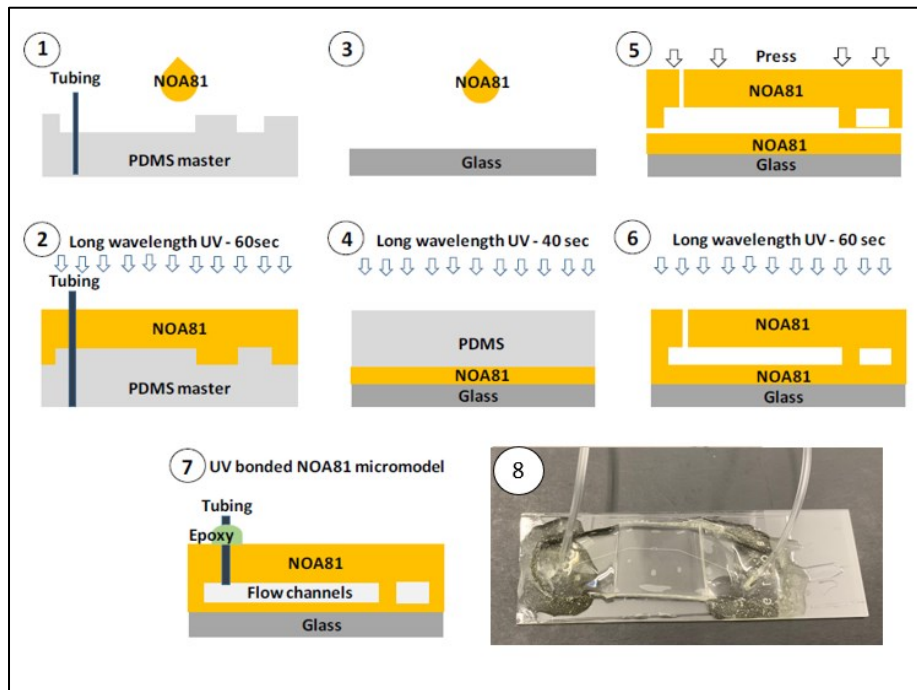


Figure 2.3.: NOA81 micromodel fabrication process. NOA81 to NOA81 half-curing bonding method.

2.3. Experimental preparation and set-up

A complete realization of the “Reservoir on a Chip” (ROC) micromodel can be achieved once the fabricated ROC is used to perform displacement experiments. In this section, we describe the experimental displacement setup and preparation of ROC.

The experimental set – up for displacement with ROC (Figure 2.4 and 2.5) includes a microscope (Olympus BX60, 5x magnification) for the visualization of oil and water phases in ‘Reservoir – on – a Chip’. The inlet and outlet of ROC are connected with tubing (FEP Tubing 1/16" OD x .010"). Reservoir fluid is collected at the outlet of the reservoir micromodel for

volumetric measurement. Oil and water are injected through a syringe (3 mL BH, Part number: BH3LS) using a syringe pump with rate 2 – 10 $\mu\text{L}/\text{min}$ (Model No: 1010, Serial No:295526, New Era Pump System Inc). For properly distinguishing the oil/water interface during fluid transport, a blue tracer dye (Spectrum, FD &C Blue #1) was mixed with deionized water. We used a digital camera (AmScope, MU1403) to record all two-phase flow experiments. Experiments under different reservoir temperatures were run using HCS321 (INSTECH) heating stage. Tubing column at outlet side was open to the atmosphere and used to measure the permeability of the system (Tygon tubing, ID = 254 μm). Pressures were measured by pressure gauges from inlet and outlet side of the system (Druck DPI 104, 5000psi sg) in kPa units (integer units, example - 51 kPa).

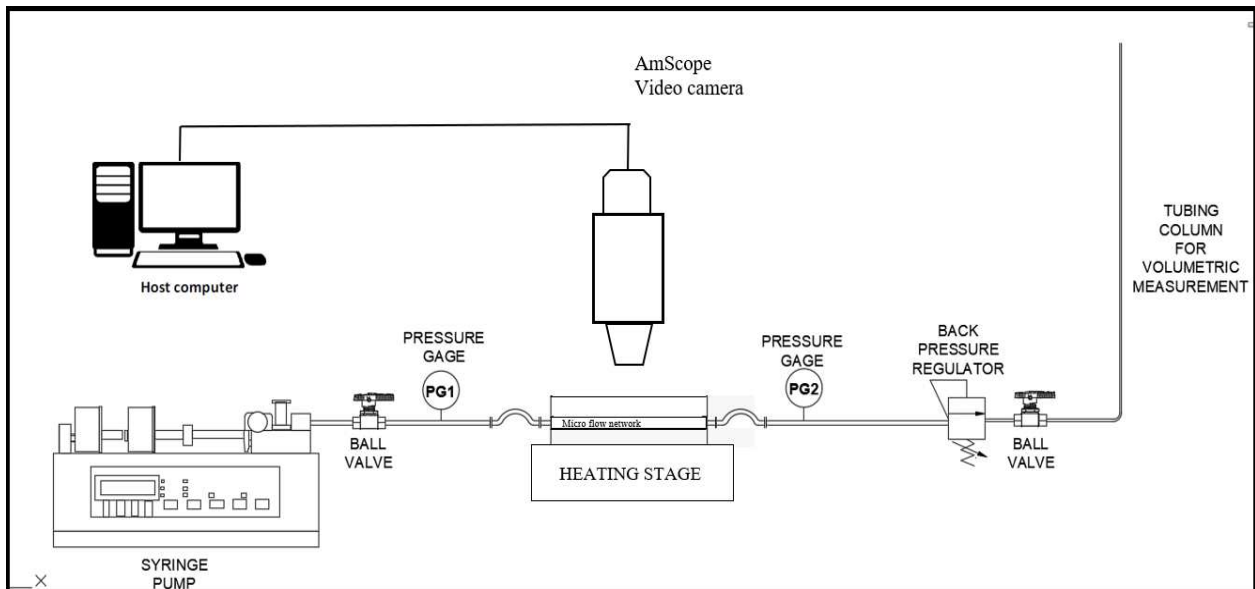


Figure 2.4.: Schematic of experimental set-up for displacement test with ROC.

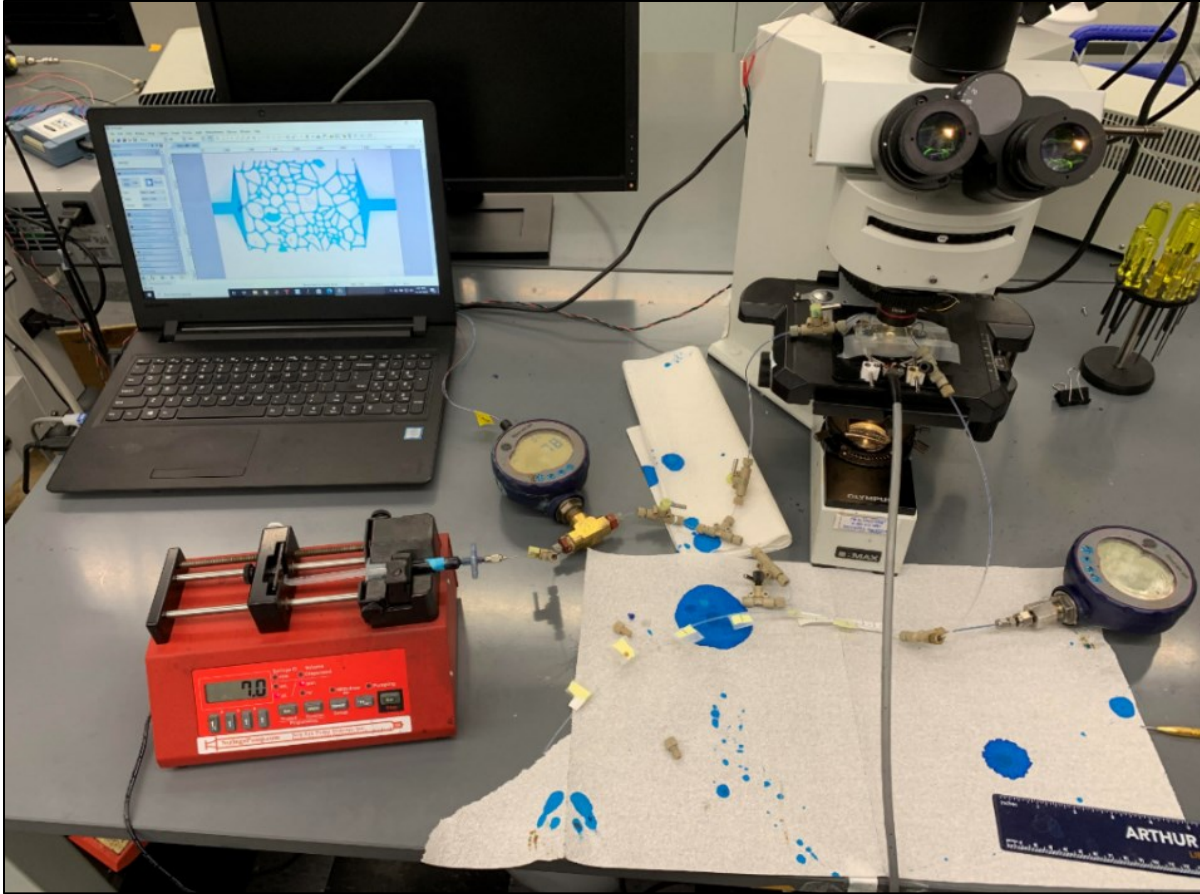


Figure 2.5: Experimental Set-up of displacement experiment with ROC.

2.4. Fluid and NOA81 Properties

In this study, we used mineral oil and deionized water for displacement tests. The viscosities of fluid were measured using capillary viscometer (Cannon-Fenske) size 50 for water and 150 for mineral oil. Figure 2.6 and 2.7 show the viscosity measurement results at different temperatures of mineral oil and water respectively.

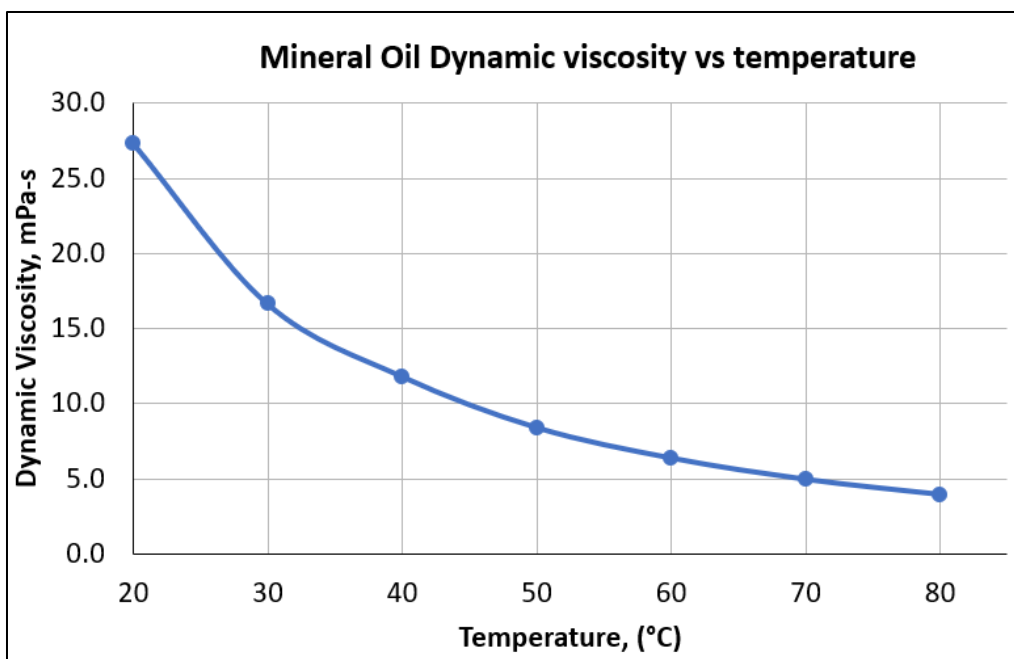


Figure 2.6: Mineral oil viscosity vs temperature.

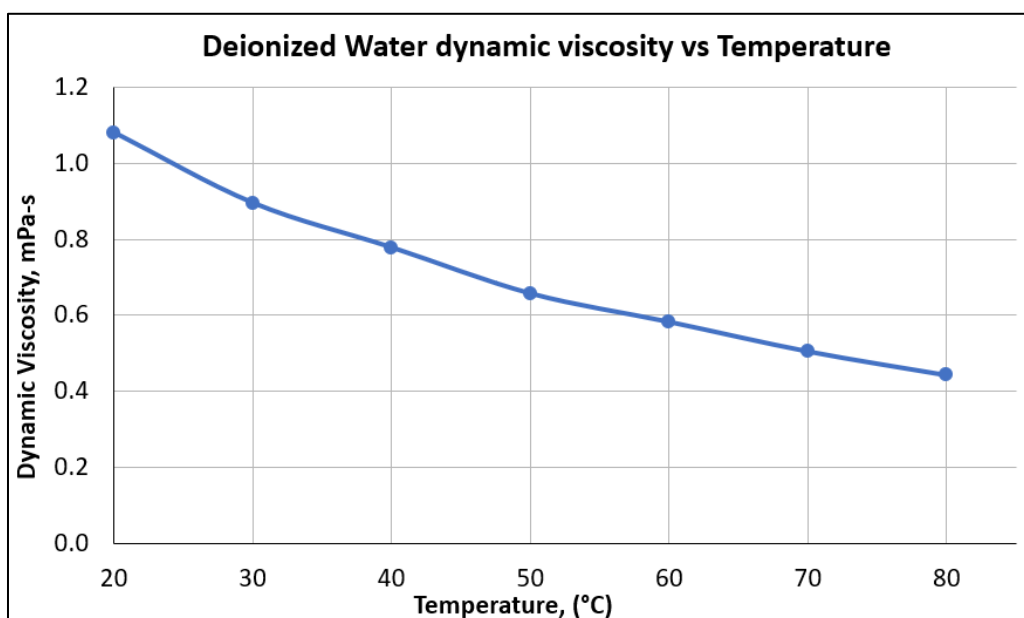


Figure 2.7: Water viscosity vs temperature.

Interfacial tension (IFT) measurements were conducted using DSA – 100 drop shape analysis. It involves suspending a droplet of the given liquid (dye water) in another liquid (mineral oil) for IFT determination. The liquid droplet is allowed to hang from a syringe tip. The size and shape of the liquid droplet is mainly a function of the prevailing IFT between deionized water and

mineral oil. From this method, the IFT values were determined from a profile (image) of the static pendant drop. Figure 2.8 shows the equilibrium shapes of water droplet at ambient (20°C), 50° and 70°C temperatures. Figure 2.9 illustrates the relationship between IFT and temperatures.

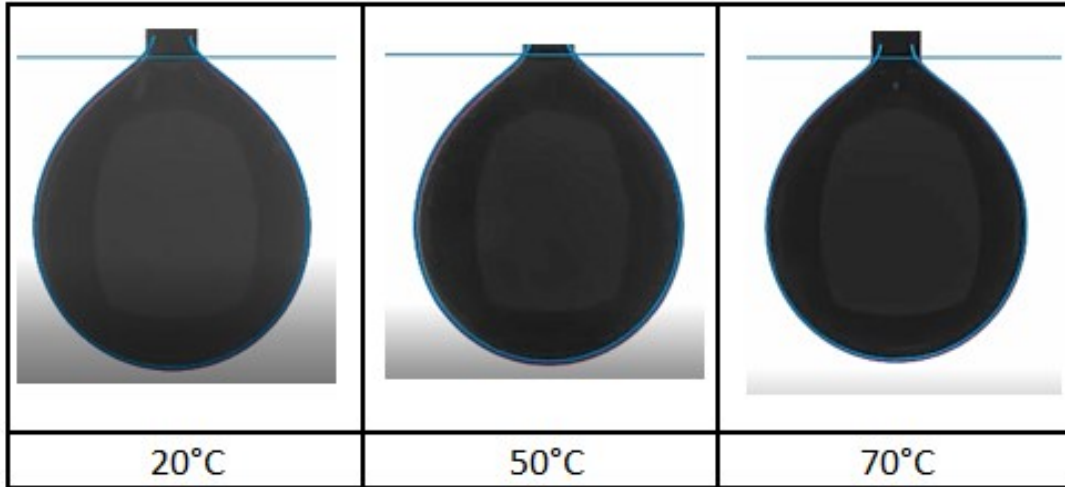


Figure 2.8: Pendant drop of water at 20°C, 50° and 70°C.

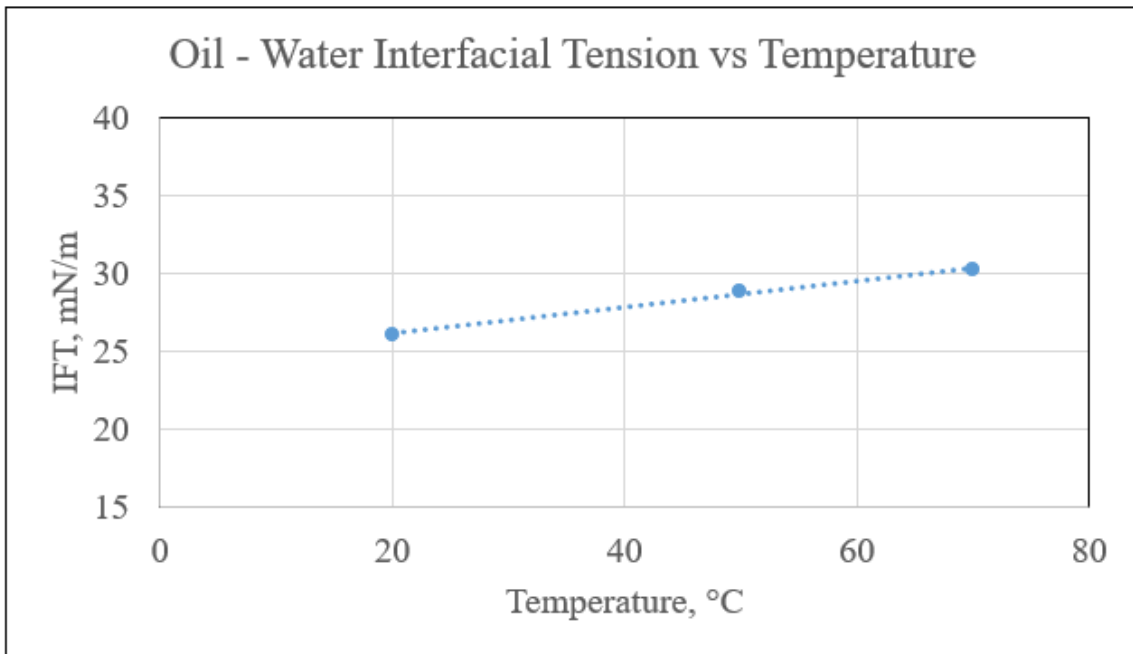


Figure 2.9: Oil – Water Interfacial Tension versus Temperature.

The effect of interfacial tension, flow velocity and viscosity on relative permeability is usually defined via a dimensionless number that relates viscous forces and capillary forces. This parameter is called capillary number, denoted by N_c and defined by:

$$N_c = \frac{\mu u}{\sigma \phi} \quad (2.1)$$

where μ is fluid viscosity, u is flow velocity, σ is the interfacial tension and ϕ is the porosity in fraction. Table 2.1 shows the capillary number for oil and water from displacement tests at different temperatures.

Table 2.1: Oil and water capillary number at different temperatures

| | temperature, [°C] | viscosity, [cp] | velocity, [m/s] | IFT, [mN/m] | porosity, [fraction] | N_c |
|-------|-------------------|-----------------|-----------------|-------------|----------------------|----------|
| Water | 20 | 1.10 | 2.94E-03 | 26.07 | 0.26 | 4.77E-04 |
| | 50 | 0.70 | 4.01E-03 | 28.85 | 0.26 | 3.75E-04 |
| | 70 | 0.56 | 5.78E-03 | 30.26 | 0.26 | 4.11E-04 |
| Oil | 20 | 28.00 | 2.20E-04 | 26.07 | 0.26 | 9.10E-04 |
| | 50 | 8.50 | 6.39E-04 | 28.85 | 0.26 | 7.24E-04 |
| | 70 | 6.00 | 1.07E-03 | 30.26 | 0.26 | 8.19E-04 |

The NOA81 wettability measurement was done by Kenzhekhanov (2016) by identifying the contact angle in water – oil environment using KRÜSS drop shape analyzer DSA – 100. DI water was used as surrounding phase in the cell and oil droplet was injected on the NOA81 surface. The pendant method was used to measure the contact angle of crude oil on the NOA81 surface surrounded by water.

Originally, NOA81 has both hydrophilic and lipophilic properties (Kenzhekhanov 2016) and it was confirmed by contact angle measurement. NOA81, without any additional treatment, illustrated intermediate wettability with water – oil contact angle of 87°.

2.5. Data Analysis

In this section, workflow of preprocessing the data obtained from experiments are explained. First, we obtain absolute permeability of NOA micromodel. Then, captured images and tests measurement are analyzed to obtain saturation and relative permeability.

2.5.1. Micromodel absolute permeability

The absolute permeability of NOA81 micromodels is estimated from single-phase flow experiments. Before the absolute permeability test, the micromodel is flooded with brine (2% KCL) as a saturation fluid for about 15 minutes to displace the air. When the micromodel is fully water-saturated (Figure 2.10), absolute permeability is measured under constant pressure. The flow rate is measured from the outlet tubing column. Since we know the flow rate, we can calculate absolute permeability using Darcy's equation:

$$q = \frac{kA \Delta p}{\mu_w L} \quad (2.2)$$

where q is the flow rate, k is the absolute permeability, A is the cross-section of the micromodel; μ_w is the water viscosity; Δp is the pressure difference between inlet and outlet sides of the micromodel, and L is the length of the micromodel.

The flow rate is calculated by:

$$q = \frac{\pi d^2 \Delta l}{4 \Delta t} \quad (2.3)$$

where d is the diameter of the measuring tube; Δl is distance between marked scales on the measuring tube; and Δt is the time interval for the meniscus in the measuring tube to pass the length of Δl . Substitution of Equation 2.2 into 2.3 gives an equation for the absolute permeability:

$$k = \frac{\pi d^2 \Delta l \mu_w * L}{4 \Delta t A \Delta p} \quad (2.4)$$

Table 2.2 shows absolute permeability calculation from experiments using Equation 2.4. As shown in Table 2.2, the absolute permeability of the micromodel measured with deionized water varies between 74.7 and 76.1 md.

Table 2.2: Absolute permeability measurements

| # of test | Pressure, Δp , [kPa] | time, Δt , [s] | Temperature, [°C] | Viscosity, [cp] | Distance, Δl , [cm] | Porosity, [fraction] | Absolute Permeability, k , [md] |
|-----------|------------------------------|------------------------|-------------------|-----------------|-----------------------------|----------------------|-----------------------------------|
| 1 | 98 | 35.1 | 20 | 0.0011 | 5.1 | 0.26 | 74.7 |
| 2 | 98 | 34.9 | 20 | 0.0011 | 5.1 | 0.26 | 75 |
| 3 | 97 | 21.35 | 50 | 0.0007 | 5 | 0.26 | 75.8 |
| 4 | 97 | 22.03 | 50 | 0.0007 | 5.1 | 0.26 | 74.9 |
| 5 | 96 | 17.48 | 70 | 0.00056 | 5 | 0.26 | 76.1 |
| 6 | 96 | 17.67 | 70 | 0.00056 | 5 | 0.26 | 75.2 |

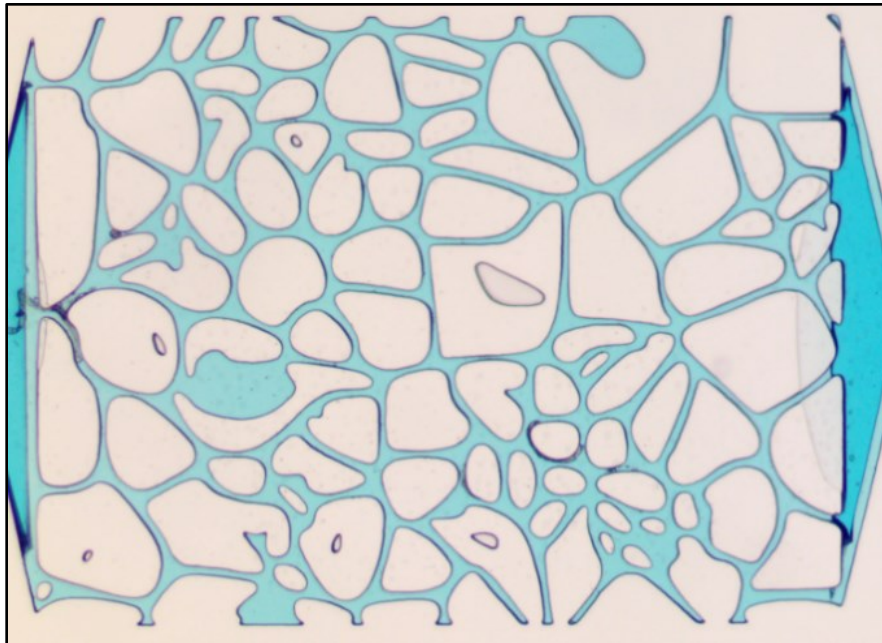


Figure 2.10: Fully water saturated micromodel, $S_w = 100\%$.

2.5.2. Data Processing from Images

In this study, primary data processing is by the analysis of images, which are captured from recorded video of the displacement experiment (Photo Capture Resolution - 4096 x 3286, Photo Capture Framerate - 6.2 fps). From the video, we captured video frames as new photos with the assistance of PhotoDirector 8. (Figure 2.11) Then, the images were preprocessed with ImageJ by transforming, rotating and cropping the area of interest (porous media) (Figure 2.12).

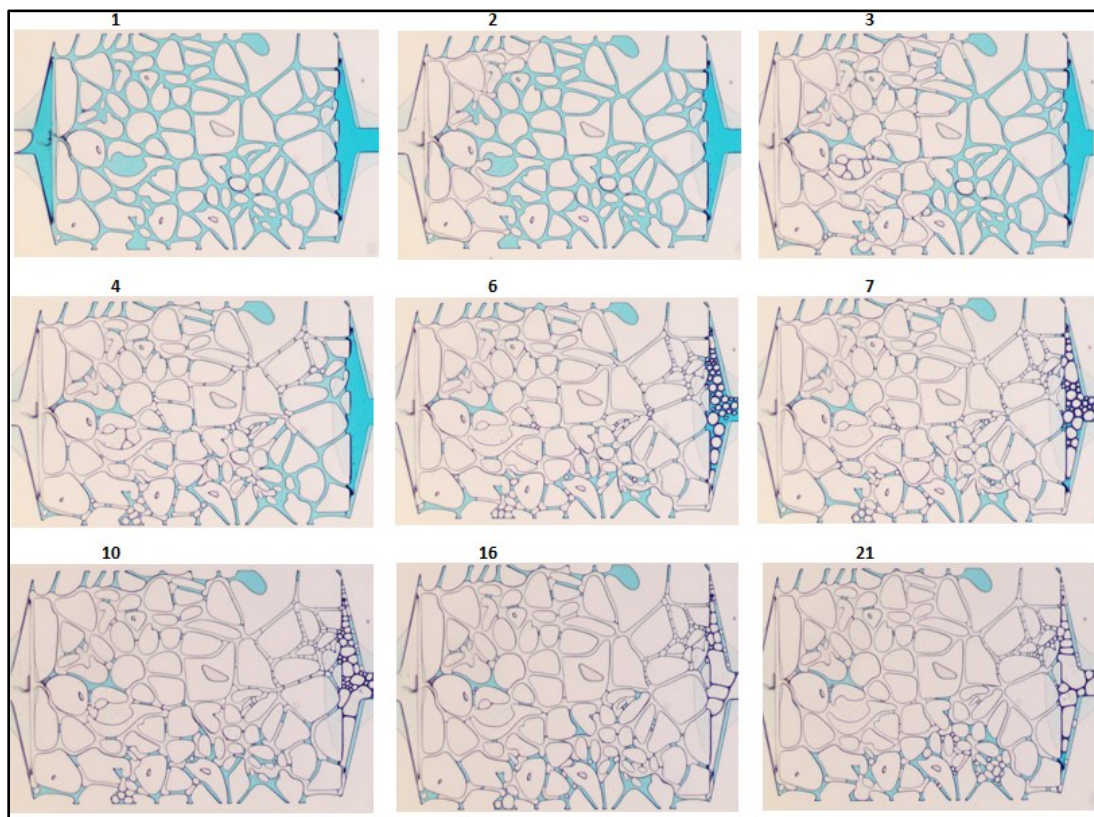


Figure 2.11: Sequence of captured images from oil-water displacement test with PhotoDirector8.

The general idea of image analysis is to separate water, oil and surrounding “rock” by threshold pixel number. All captured images were converted into binary black/white images with the assistance of MATLAB and its Image Processing Toolbox. MATLAB can provide basic data processing and Image Processing Toolbox and has many useful built-in scripts for image enhancement, image segmentation and object detection.

Water with fluorescent dye is a white region while oil and rock are black (Figure 2.13). In order to determine the water saturation from images, the ratio of quantity of white pixels at certain image at time t to the quantity of white pixels when system was fully water saturated at time t_0 , represents the water saturation at time t (Equation 2.5).

$$S_w@t = \frac{NW@t}{NW@t_0(S_w=100\%)} \quad (2.5)$$

where $S_w@t$ is water saturation at certain time t , $NW@t$ is the number of white pixels representing water quantity at time t , $NW@t_0$ is the number of white pixels at t_0 , when system was fully water saturated ($S_w = 100\%$). An example of water saturation determination is shown in Figure 2.17.

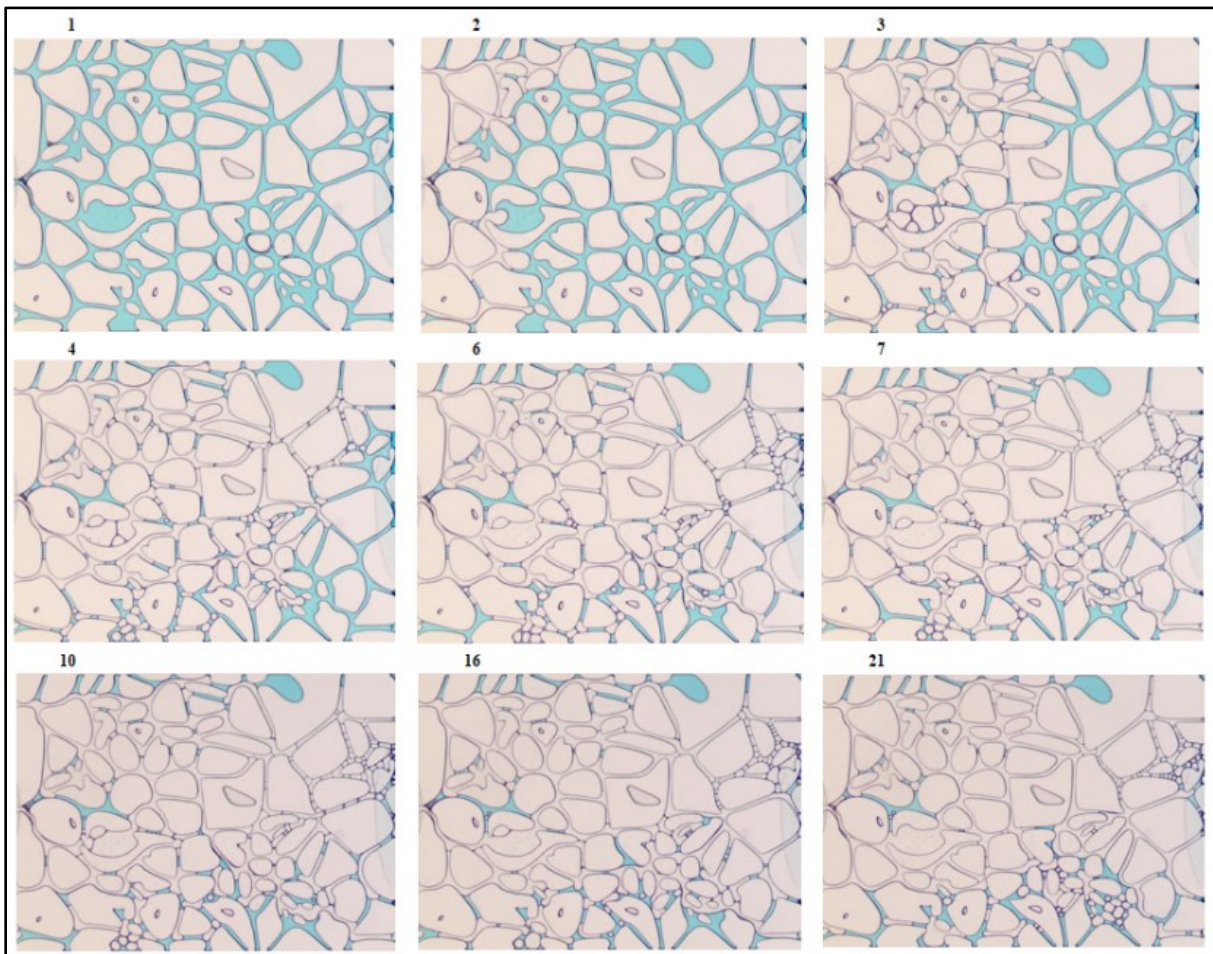


Figure 2.12: Preprocessed sequence of images from oil – water displacement test with ImageJ.

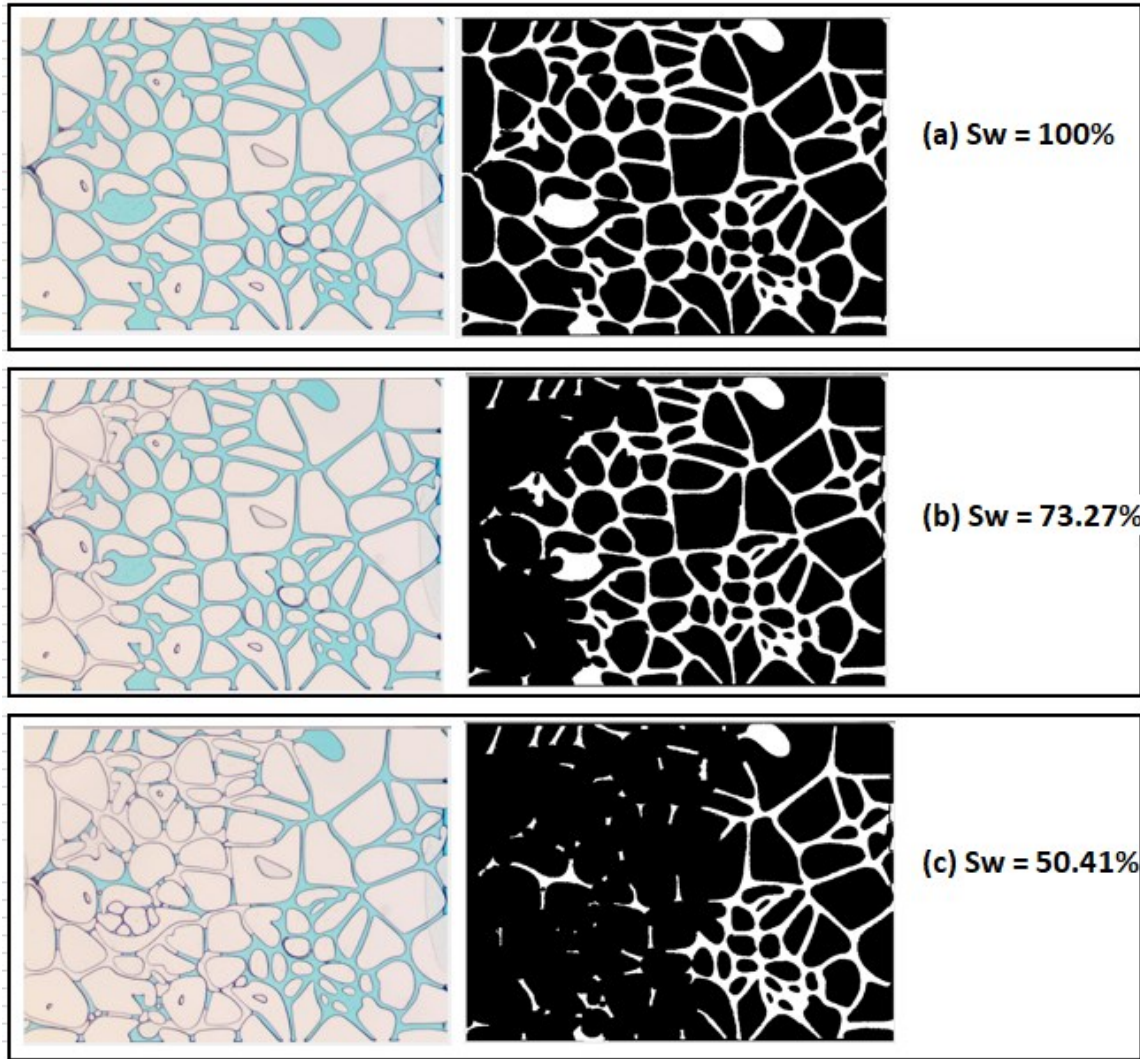


Figure 2.13: Water saturation determination from binary images (a) at fully water saturated, (b) water saturation = 73.27% and (c) at 50.41% water saturation.

The same procedures were followed to obtain water saturation over time in water – oil displacement tests. Figure 2.14 illustrates the image sequence obtained from a water – oil displacement experiment. Water saturation relationship versus cumulative water injection quantity in PV is shown in Figure 2.15.

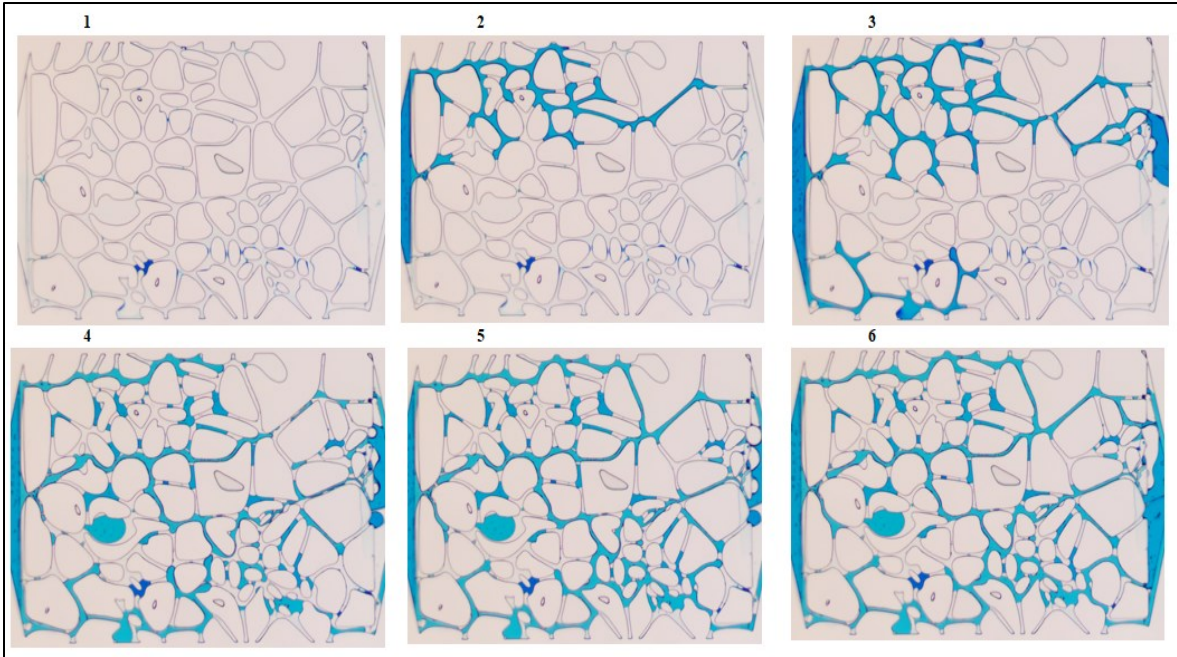


Figure 2.14: Image sequence of water-oil displacement test.

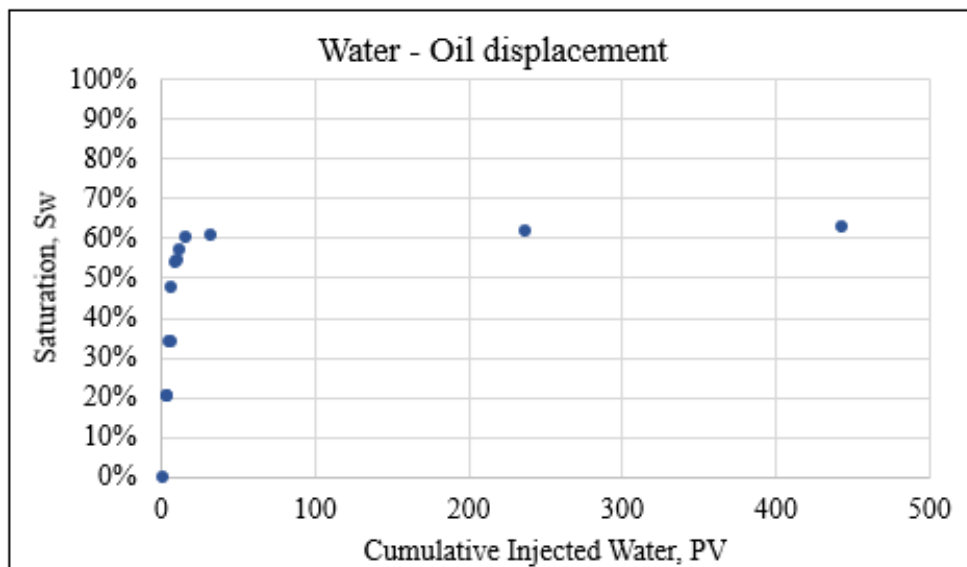


Figure 2.15: Water saturation vs Cumulative Water Injection in PV unit.

Pore Volume (PV) is a dimensionless time scale. Unit PV is the time when Injected fluid volume equals to the total pore volume (Equation 2.6).

$$1PV = \frac{\text{time (s)} * \text{flowrate} \left(\frac{m^3}{s} \right)}{\text{total Pore Volume (m}^3\text{)}} \quad (2.6)$$

2.5.3. Relative permeability

In this study, two methods for estimating relative permeabilities from displacement data are used. The first one is the Jones and Roszelle (1978) method. The second is the alternative method based on Darcy's equation (the DE method).

Relative permeability Estimation by the Extended form of JBN (Jones and Roszelle) method

The method, proposed by Jones and Roszelle (1978), is used to calculate relative permeability of the system. Ignoring gravity effects and capillary pressure, water and oil relative permeabilities (expressed as function of saturation) are given by

$$k_{rw} = \frac{\mu_w f_{w2}}{\lambda_2^{-1}} \quad (2.7)$$

and

$$k_{ro} = \frac{\mu_o f_{o2}}{\lambda_2^{-1}} \quad (2.8)$$

To use these equations, the fractional flow of water and oil and effective viscosity, λ^{-1} , must be determined as a function of saturation. The most common determination location is the outlet end of the core where the fractional flow is the same as the produced oil or water cut. Average water saturation was obtained by initial water saturation and injected water volumes converted into pore volumes, Q_i :

$$\bar{S}_w = S_{wi} + \frac{N_p}{PV} \quad (2.9)$$

Saturation at the outlet of the system is

$$S_{w2} = \bar{S}_w - Q_{wi} \frac{d\bar{S}_w}{dQ_{wi}} \quad (2.10)$$

Fractional flow of oil is, then, calculated from the average and outlet water saturations by

$$f_{o2} = \frac{\bar{S}_w - S_{w2}}{Q_{wi}} \quad (2.11)$$

Also,

$$f_{w2} = 1 - f_{o2} \quad (2.12)$$

By definition, the effective viscosity (reciprocal relative mobility) at any point in a linear core is

$$\lambda^{-1} = \frac{kA}{q} \left(\frac{dp}{dl} \right) \quad (2.13)$$

But,

$$kA = \frac{q_b \mu_b L}{-\Delta p_b} \quad (2.14)$$

where $-\Delta p_b$ is the pressure drop across the entire core during the single-phase flow of a fluid of viscosity μ_b at rate q_b , for example, during absolute permeability determination. Also, since

$$l = xL \quad (2.15)$$

then

$$\lambda^{-1} = \left(\frac{q_b \mu_b}{\Delta p_b} \right) * \frac{1}{q} * \left(\frac{dp}{dx} \right) \quad (2.16)$$

$$\lambda_2^{-1} = \lambda^{-1} - Q_{wi} \frac{d\lambda^{-1}}{dQ_{wi}} \quad (2.17)$$

Relative permeability from image processing (DE method)

In this method, we obtained relative permeability of displaced fluid using Darcy's equation. After absolute permeability measurement, we started injecting oil to displace the water from the porous media until irreducible water saturation was reached. At that point, we measured the oil relative permeability at the endpoint ($k_{ro}@ S_{wr}$) using Darcy Eq. by measuring flow rate from the outlet of the system. Eventually, from oil – water displacement test we obtained water relative permeabilities from image processing, irreducible water saturation point and oil relative permeability at S_{wr} .

Next, we started injecting water to displace the oil from the system. In this case, oil was displaced fluid, so we were able to obtain oil relative permeability data from image processing. When we reached residual oil saturation point, we calculated water relative permeability at residual oil saturation ($k_{rw}@ S_{or}$). Consequently, from water – oil displacement test, we obtained the oil relative permeability data from image processing, residual oil saturation point and water relative permeability at S_{or} .

Despite the fact that water relative permeability data obtained from oil – water displacement test started from fully water saturation system ($k_{rw} = 1 @ Sw = 100\%$), we plotted the oil and water relative permeability data at saturations between irreducible water saturation and residual oil saturation. Consequently, the relative permeability data at saturations below irreducible water saturation and above residual oil saturation were ignored in the analysis.

As noted earlier, determination of relative permeability of displaced fluid from displacement experiment is based on Darcy's equation:

$$v_s = \frac{k_r k}{\mu_d} * \frac{\Delta p}{L} \quad (2.18)$$

where v_s is superficial velocity and k_r is relative permeability of the displaced fluid, k is the absolute permeability A is the cross section of the porous medium, μ_d is the viscosity of displaced fluid and Δp is the pressure difference between the inlet and outlet of porous medium.

Saturation of displaced fluid as a function of time is required to calculate the volumetric rate of the displaced fluid. Afterwards, the volume of the displaced fluid between times t_1 and t_2 are calculated by

$$V_{produced} = PV * (S_{t1} - S_{t2}) \quad (2.19)$$

where $V_{produced}$ is the volume of the displaced fluid, PV is the pore volume of the porous medium, and $S_{t1} - S_{t2}$ is the saturation difference between times t_1 and t_2 . Then, the velocity of the displaced fluid between times t_1 and t_2 is obtained from

$$v_d = \frac{V_d}{t_2 - t_1} * \frac{1}{D * W * \emptyset} \quad (2.20)$$

where D is the depth and W is the width of the porous medium, which are 15 μm and 850 μm respectively for the particular setup used in this research.

The superficial velocity between two time points (t_2 and t_1) is given by

$$v_s = v_d * \frac{S(t_1) - S(t_2)}{2} \quad (2.21)$$

Consequently, using the superficial velocity, the relative permeability is estimated from

$$k_r = \frac{\mu_d * v_s * L}{k \frac{[\Delta p(t_1) + \Delta p(t_2)]}{2}} \quad (2.22)$$

The procedure explained above allows to calculate the relative permeability of the displaced fluid. We performed oil – water and water – oil displacement experiments to obtain the

relative permeability for both oil and water in displacement experiments. Water and oil relative permeabilities at the end points (irreducible water, S_{wr} , and residual oil, S_{or} , saturations, respectively) are found from Darcy's equation at the end of the displacement test.

The end point water relative permeability at residual oil saturation is obtained from

$$k_{rw} = \frac{\mu_w * q * L}{k * A * \Delta p} \quad (2.23)$$

where μ_w is the water viscosity and q is the volumetric flow rate. Similarly, the end point oil relative permeability at the irreducible water saturation is given by

$$k_{or} = \frac{\mu_o * q * L}{k * A * \Delta p} \quad (2.24)$$

where μ_o is the water viscosity and q is the volumetric flow rate.

CHAPTER 3

EXPERIMENTAL RESULTS AND ANALYSIS

3.1. Relative Permeability using Darcy Equation method

In this section we present relative permeability estimations from two-phase displacement experiments through Image processing procedure by the DE method. Water saturation of captured images from displacement tests is determined by converting images to binary images, where white pixels represent water quantity and black pixels represent oil and “rock”, and the ratio of the number of white pixels at a certain time to the number of white pixels at $S_w = 100\%$ gives the water saturation at that time. Example below shows an oil – water displacement experiment conducted at 50°C .

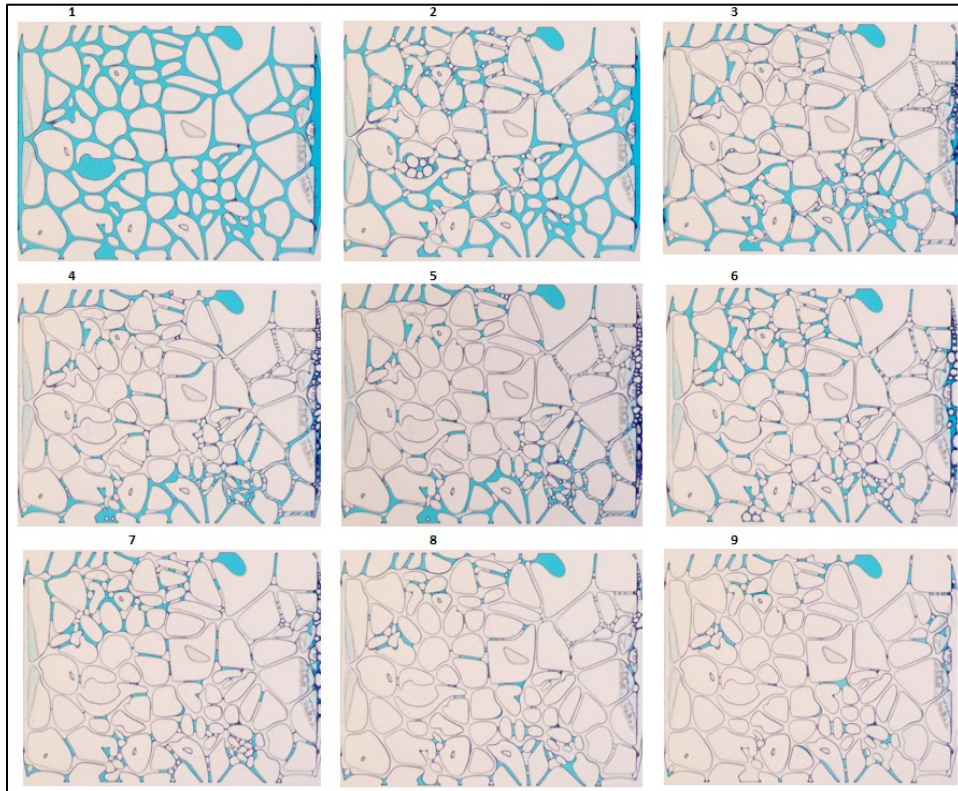


Figure 3.1: Image consequences from an oil – water displacement test conducted at 50°C .

After image processing and data analysis, we plotted the saturation versus time of the oil – water displacement test. Figure 3.2 shows the water saturation profile vs time and Figure 3.3 shows the saturation vs Cumulative Injected oil in PV. From the saturation profile, it is possible to determine when the oil reached the outlet of porous medium, which is the time when the gradient of saturation versus time, $\left| \frac{dS_w}{dt} \right|$, dramatically decreased (approximately one-third of a second).

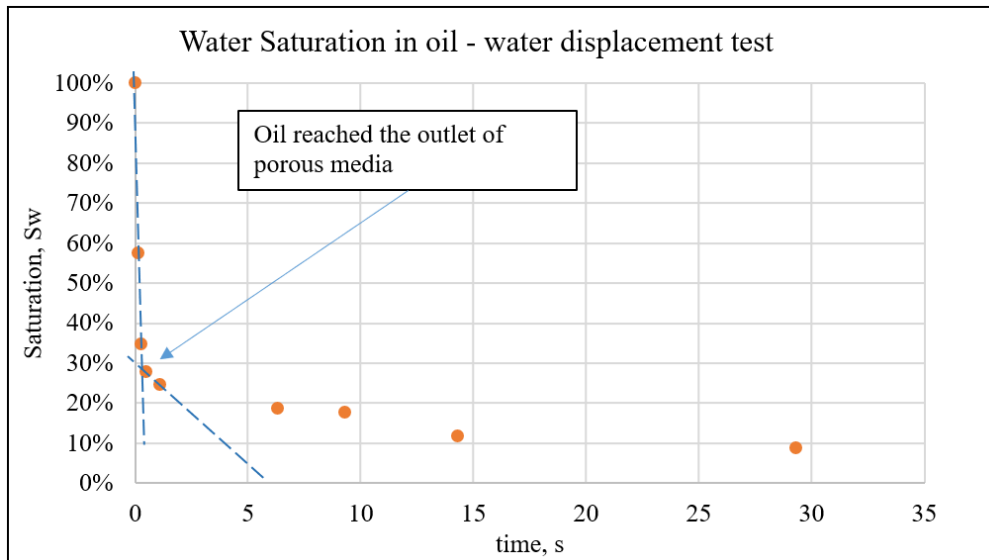


Figure 3.2: Saturation vs time in oil-water displacement test.

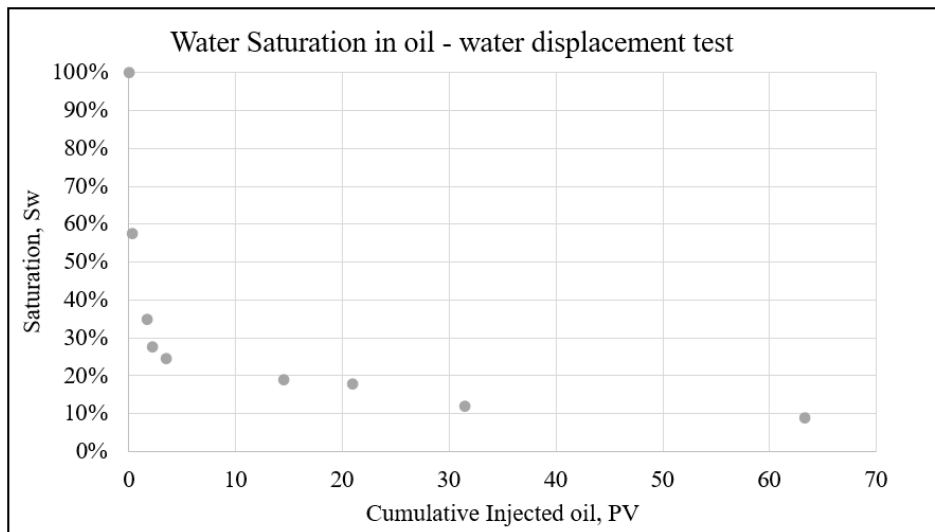


Figure 3.3: Saturation vs Cumulative PV Injection of oil.

After preprocessing the data from oil-water displacement test and obtaining saturation profile, we used Equations 2.17 – 2.23 to calculate the relative permeability of the displaced fluid (water in this case). Table 3.1 shows the result of water relative permeability calculation using the DE method. As shown in Table 3.1, oil – water displacement process was conducted at constant injection pressure, and the water relative permeabilities were plotted in Figure 3.4.

Table 3.1: Relative water permeability calculation the DE method

| Saturation, S_w , [%] | Pressure, P, [kPa] | Volume of displaced fluid, [m ³] | Velocity of displaced fluid, [m/s] | Superficial velocity, [m/s] | Relative water permeability, k_{rw} , [fraction] |
|-------------------------|--------------------|--|------------------------------------|-----------------------------|--|
| 100% | 84 | 0 | 0 | 0 | |
| 65% | | | | | 0.6000 |
| 58% | 84 | 1.59E-12 | 4.35E-03 | 4.35E-03 | 0.5935 |
| 35% | 84 | 8.47E-13 | 1.96E-03 | 3.16E-03 | 0.4303 |
| 28% | 84 | 2.62E-13 | 3.64E-04 | 1.16E-03 | 0.1583 |
| 25% | 84 | 1.23E-13 | 6.11E-05 | 2.12E-04 | 0.0290 |
| 19% | 84 | 2.14E-13 | 1.24E-05 | 3.67E-05 | 0.0050 |
| 18% | 84 | 3.75E-14 | 3.77E-06 | 8.07E-06 | 0.0011 |
| 12% | 84 | 2.25E-13 | 1.36E-05 | 8.66E-06 | 0.0012 |
| 9% | 84 | 1.12E-13 | 2.26E-06 | 7.91E-06 | 0.0011 |

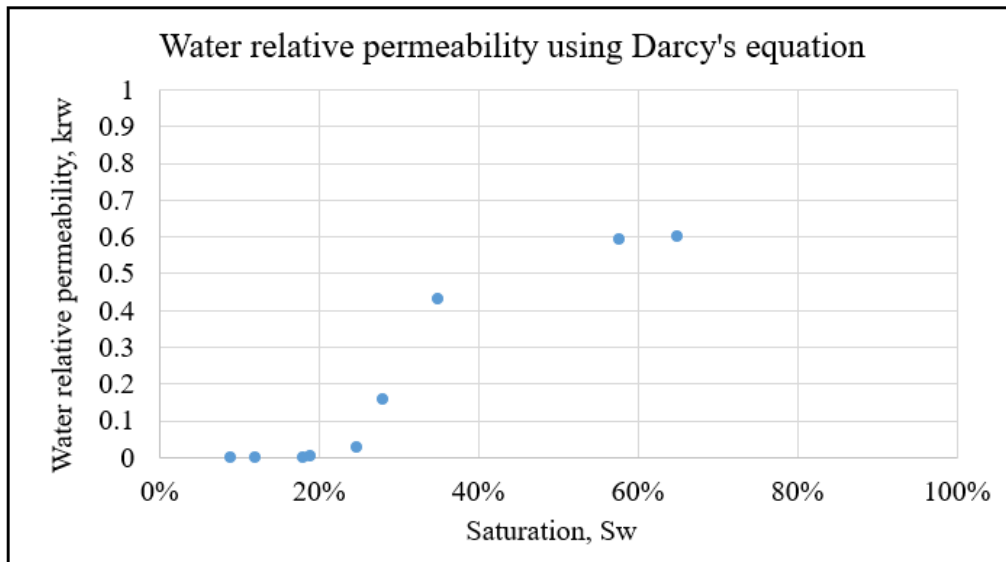


Figure 3.4: Water relative permeability using the DE method.

Next, we started injecting water and replaced the oil from system in order to calculate oil relative permeability. Figure 3.5 illustrates the captured images that represent water – oil displacement process conducted at 50°C temperature condition.

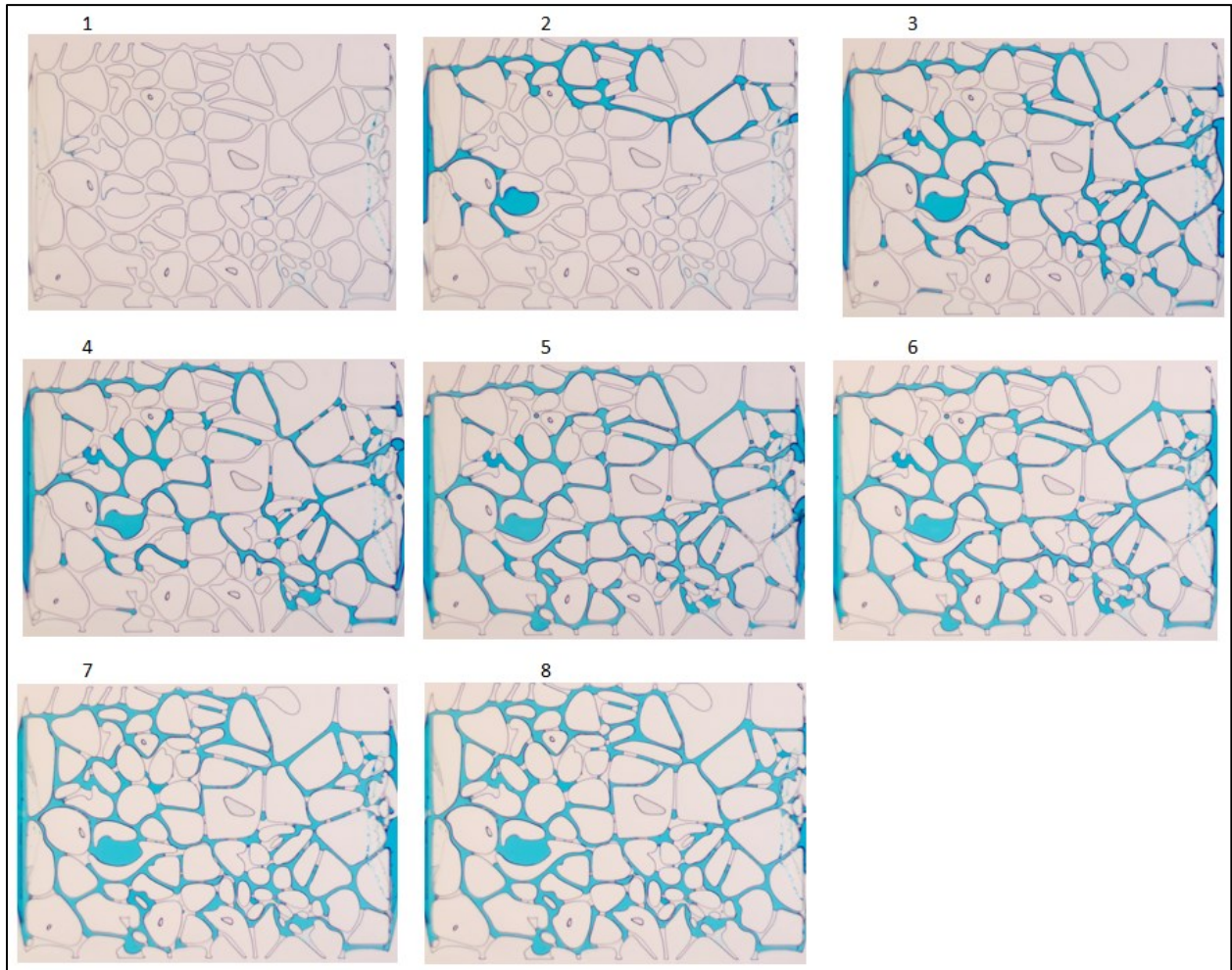


Figure 3.5: Image sequence from water – oil displacement test at 50°C.

Processing and analysis of captured images were accomplished with the assistance of MATLAB Image Processing Toolbox, (by constructing the binary images, where white pixels represent water, and black – oil and ‘solid grains’). The quantity of white pixels at each time step (image) were divided by the quantity of white pixels at $S_w = 100\%$ (measured absolute permeability) and provided the saturation at each time step (or image). The saturation profile versus time and cumulate injected water are shown in Figures 3.6 and 3.7, respectively.

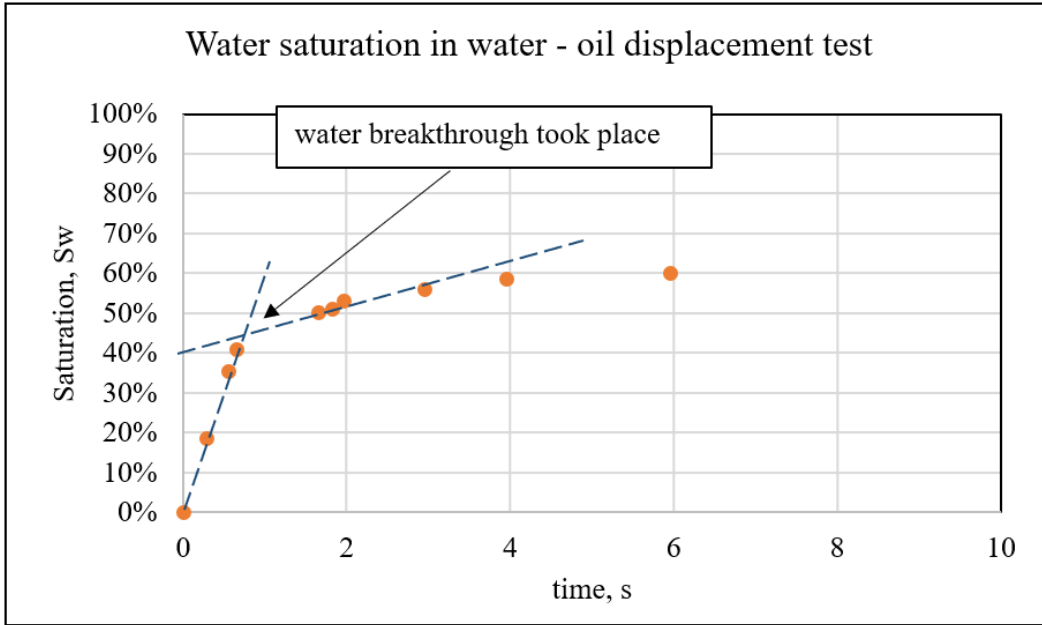


Figure 3.6: Water saturation profile versus time in water – oil displacement test at 50°C.

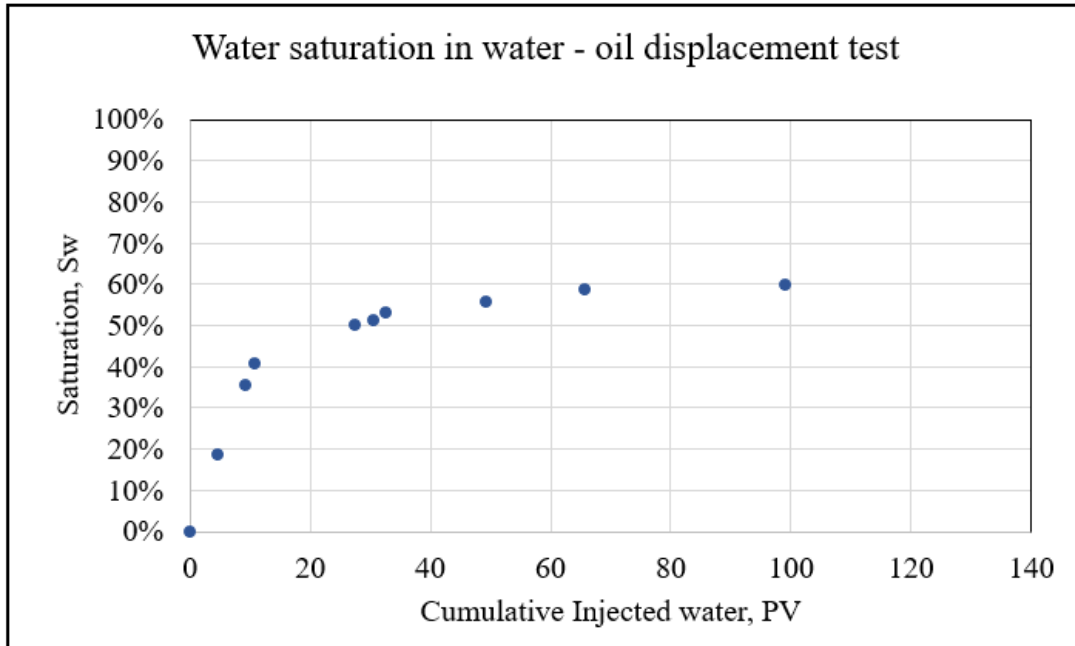


Figure 3.7: Water saturation versus Cumulative injected water in pore volume.

Conducting the same analysis as we did with saturation profile of oil – water displacement test, water breakthrough took place around 0.65 seconds after water invading porous medium. Utilizing the DE method and using Equations 2.18 – 2.24, we calculated the relative permeability

of oil. Table 3.2 presents the result of analysis. The experiment was conducted at constant pressure and the relationship of oil relative permeability versus saturation is plotted in Figure 3.8.

Table 3.2: Relative oil permeability calculation by the DE method

| Saturation, S_w , [%] | Pressure, P , [kPa] | Volume of displaced fluid, [m ³] | Velocity of displaced fluid, [m/s] | Superficial velocity, [m/s] | Relative oil permeability, k_{ro} , [fraction] |
|-------------------------|-----------------------|--|------------------------------------|-----------------------------|--|
| 18.56% | 99 | 6.95E-13 | 7.49E-04 | 7.49E-04 | 0.818 |
| 35.56% | 99 | 1.33E-12 | 7.31E-04 | 1.48E-03 | 0.798 |
| 41.02% | 99 | 2.04E-13 | 6.17E-04 | 6.74E-04 | 0.674 |
| 50.18% | 99 | 3.43E-13 | 1.03E-04 | 3.60E-04 | 0.393 |
| 51.16% | 99 | 3.68E-14 | 6.38E-05 | 8.36E-05 | 0.091 |
| 58.72% | 99 | 1.02E-13 | 3.07E-05 | 3.14E-05 | 0.034 |
| 60.00% | 99 | 4.79E-14 | 7.23E-06 | 1.90E-05 | 0.021 |

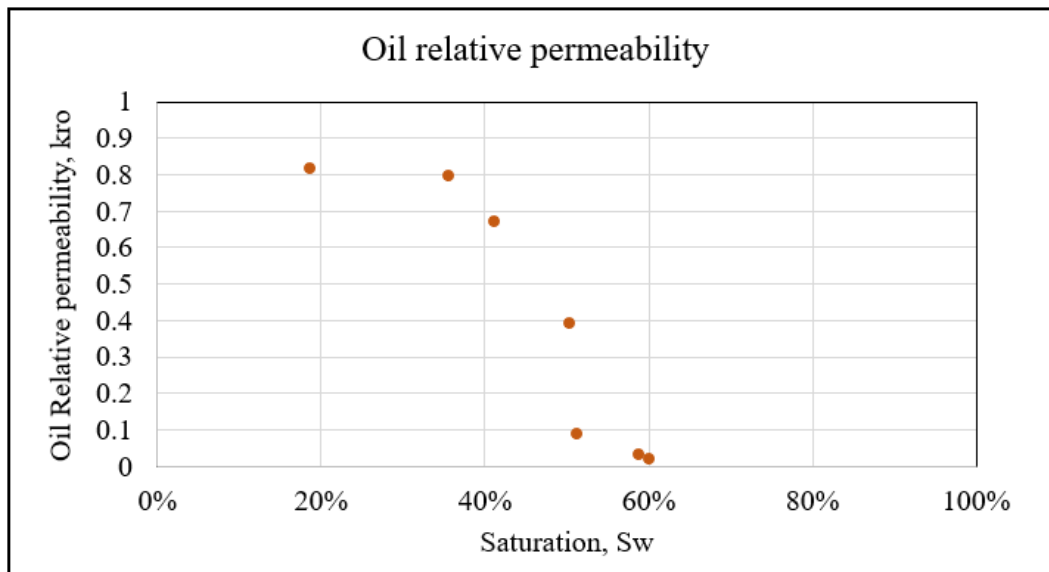


Figure 3.8: Oil relative permeability using the DE method.

3.2. Relative Permeability using the Jones and Roszelle method.

Here we present an example of oil and water relative permeability calculation from water displacing oil test using the Jones and Roszelle method. From the image sequence and saturation

data obtained before (Figures 3.5 – 3.7), we continued to process the data by using Equations 2.6 - 2.16. The parameters used and the results are presented in Table 3.3. Figure 3.10 shows the relationship of calculated oil and water relative permeabilities versus saturation. The only way to measure injection rate at the different timestep using current setup is from the outlet of the system. The displacement process occurred very fast because of small pore volume of system, so we were able to obtain only one value of injection rate, and this value were assumed constant for all timesteps.

Table 3.3: Oil and water relative permeabilities using the Jones and Roszelle method

| t, [sec] | P, [kPa] | Sw, [%] | Cumulative Injected water Qi, [PV] | Cumulative Produced oil Np, [m ³] | Cumulative Injected water Wi, [m ³] | Oil fractional flow at the outlet fo2, [fraction] | Water fractional flow at the outlet fw2, [fraction] | kro, [fraction] | krw, [fraction] |
|----------|----------|---------|------------------------------------|---|---|---|---|-----------------|-----------------|
| 0.000 | 99 | 0 | 0.00 | 0.00E+00 | 0.00E+00 | | | | |
| 0.130 | 99 | 18.6 | 2.16 | 7.03E-13 | 8.09E-12 | 0.086 | 0.914 | 0.765 | 0.536 |
| 0.300 | 99 | 41.0 | 4.99 | 1.55E-12 | 1.87E-11 | 0.079 | 0.921 | 0.708 | 0.540 |
| 1.652 | 99 | 50.2 | 27.46 | 1.90E-12 | 1.03E-10 | 0.004 | 0.996 | 0.036 | 0.584 |
| 1.826 | 99 | 51.2 | 30.35 | 1.94E-12 | 1.14E-10 | 0.003 | 0.997 | 0.030 | 0.585 |
| 3.956 | 99 | 58.7 | 65.76 | 2.23E-12 | 2.46E-10 | 0.002 | 0.998 | 0.019 | 0.586 |
| 5.956 | 99 | 60.0 | 99.00 | 2.27E-12 | 3.71E-10 | 0.000 | 1.000 | 0.003 | 0.587 |

However, obtaining both oil and water relative permeabilities, particularly the relative permeability of the displacing fluid, from water – oil displacement experiment in micromodels is challenging. The issue is the significant difference between the injection rate and the pore volume of the medium, which equals to:

$$\text{Injection rate} = 16.6 * \text{Pore Volume}$$

Figure 3.9 shows the relationship between cumulative water injection and cumulative produced oil versus time. The consequence of it is the absence of water relative permeability transition from irreducible water saturation to the saturation when relative permeability reaches a plateau. In our

example, we had a gap of water relative permeability data between 0 and 18.5% water saturation. This leads to the poor estimation of the water oil relative permeability.

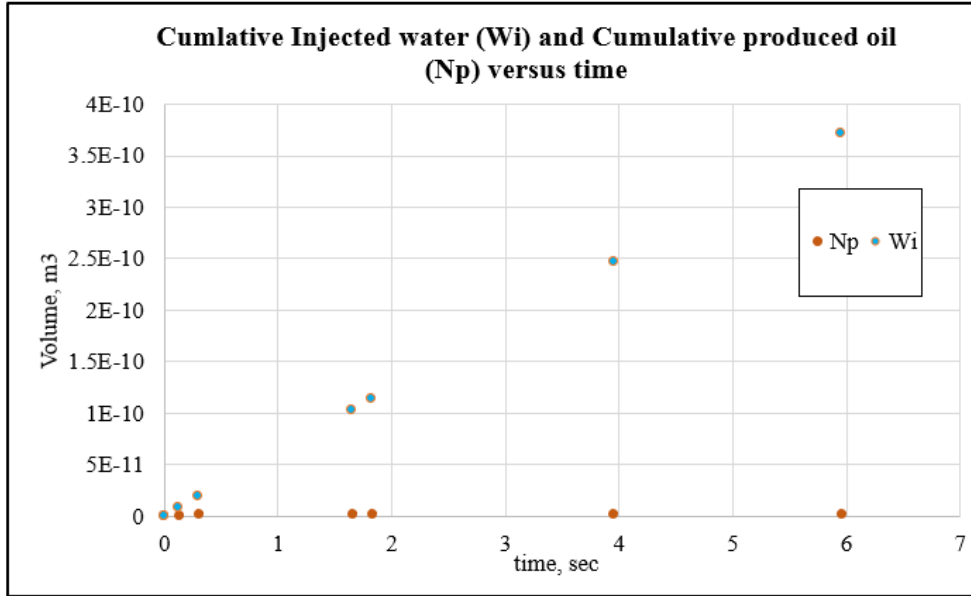


Figure 3.9: Cumulative injected water and produced oil versus time in water – oil displacement experiment.

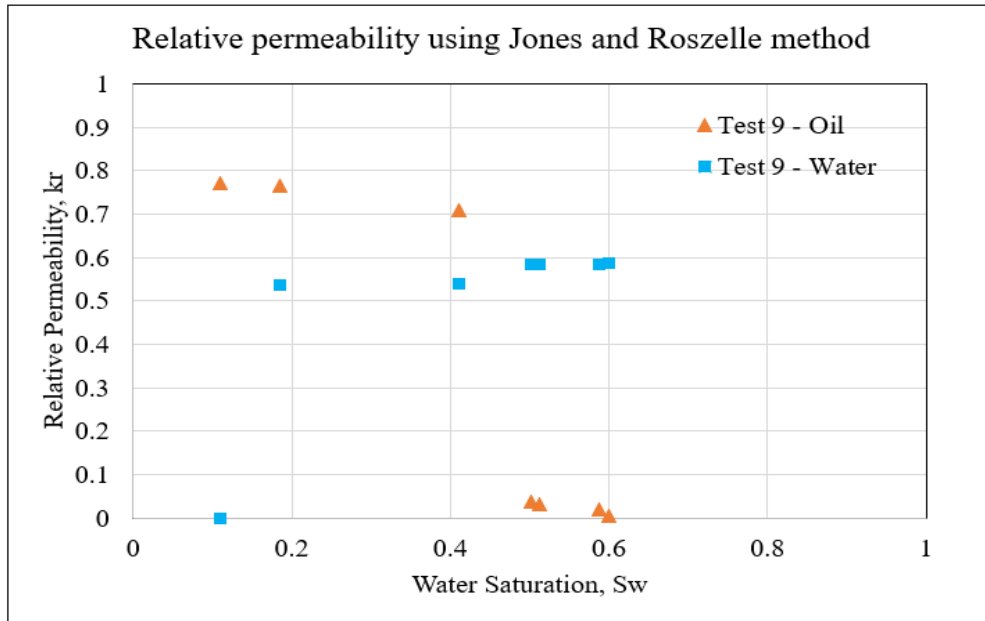


Figure 3.10.: Relative permeability based on the Jones and Roszelle method.

3.3. Effect of Temperature on oil/water relative permeability

In this section, we perform the analysis of the relative permeability results at the ambient (20°C), 50°C and 70°C temperature conditions. Even though oil and water relative permeability curves obtained separately using DE method, we compiled curves together.

We conducted 12 tests in total (oil displacing water and water displacing oil) to study the effect of temperature on oil and water relative permeabilities. Successful measurements are presented in Figures 3.11 to 3.16. Although water relative permeability data obtained from oil – water displacement test started from fully water saturation system ($k_{rw} = 1 @ S_w = 100\%$), Figure 3.11, 3.13 and 3.15 present the oil and water relative permeability data at saturations between irreducible water saturation and residual oil saturation. The relative permeability data at saturations below irreducible water saturation and above residual oil saturation were ignored in the analysis.

Some tests results are missing in these figures mainly because we did not obtain appropriate data. The main reason was that the network path was partially blocked by impurities from injected fluids.

Oil and water relative permeabilities at ambient temperature

Figure 3.11 shows the results of oil and water relative permeabilities using DE method. The shift of oil relative permeability from around 0.9 to 0.1 took place at a water saturation between 0.1 and 0.5 and the gradient of the inverse decrease is close to -1/2. While the relative permeabilities in the figure were obtained from captured images, the end points were obtained from laboratory measurements using volumetric displacement rate, i.e., at the irreducible water and residual oil saturations. Irreducible water saturations were quite consistent around 10% and

residual oil saturations were around 46%. A sharp increase of water relative permeability occurred after water breakthrough at a saturation around 40%, and the relative permeability was quite consistent at the residual oil saturation, $k_{rw} = 0.6$.

Figure 3.12 illustrates oil and water relative permeability curves obtained using the Jones and Roszelle method. Similar behavior of oil permeability curves might be observed using the Jones and Roszelle method as well as using the DE method. However, the water permeability curve from the Jones and Roszelle method does not match that from the DE method. More accurate data were obtained by the DE method mainly because of the water was displaced phase, while in the Jones and Roszelle method, water was the displacing phase. The high injection rate in comparison with the pore volume does not allow the calculation of the transition of water relative permeability.

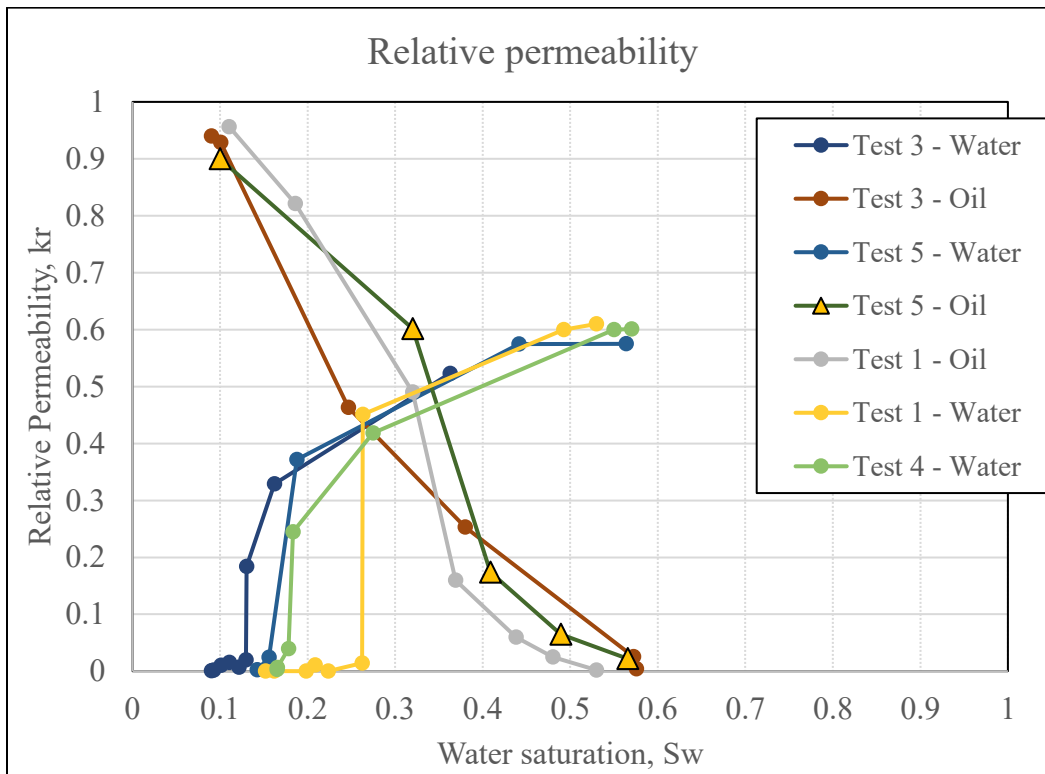


Figure 3.11: Oil and water relative permeabilities at ambient temperature using the DE method.

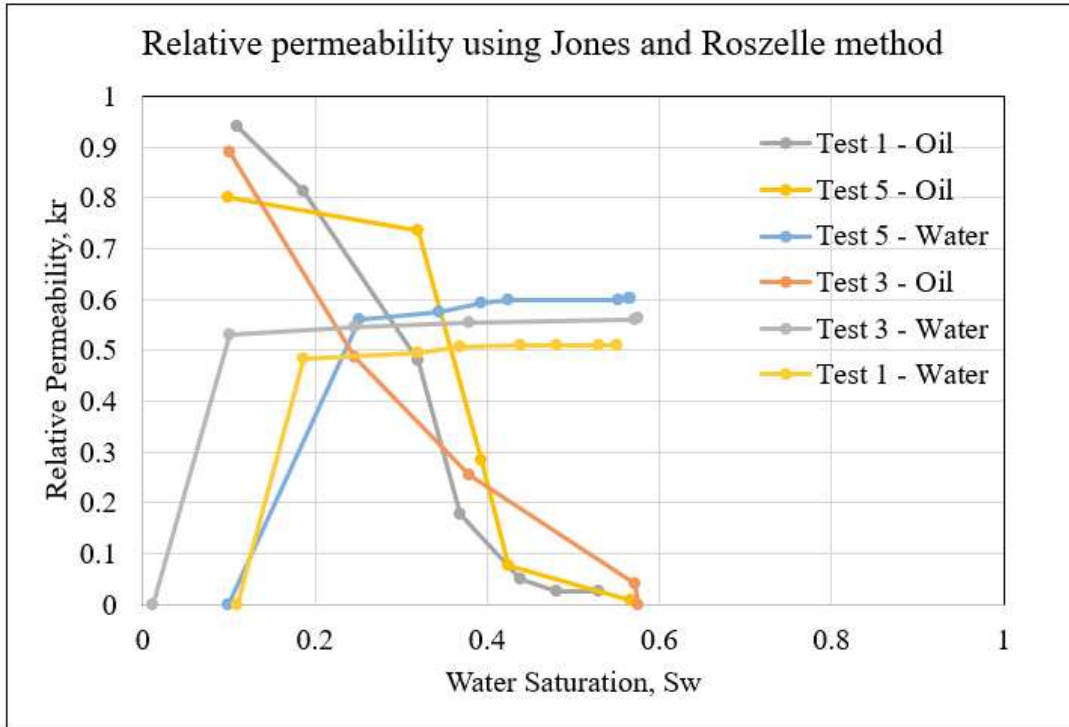


Figure 3.12: Oil and water relative permeability at ambient temperature using the Jones and Roszelle method.

Oil and water relative permeabilities at 50°C

Figure 3.13 shows the oil and water relative permeability curves obtained by the DE method at 50°C. The transition of oil permeability from around 0.8 to 0.1 occurred quicker in this case (water saturation from 30% to 50%) than it was at the ambient temperature. Residual oil saturation shifted slightly to the right (to 40%) while irreducible water saturation did not change when the temperature increased from 20° to 50°C.

The same poor quality of water permeability estimates was observed from irreducible water saturation to around 50%. The reason was the same: water was displacing phase and injection rate is very high compared to the pore volume. Oil and water relative permeabilities at end points were the same, about 0.8 and 0.6 respectively.

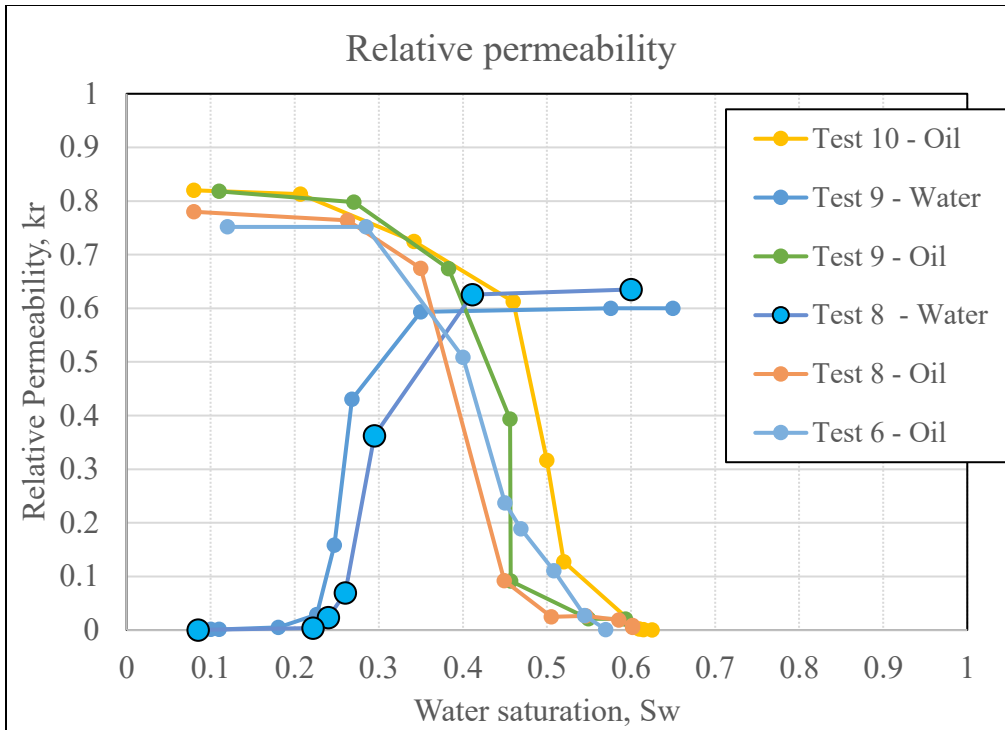


Figure 3.13: Oil and water relative permeabilities at 50° temperature using the DE method.

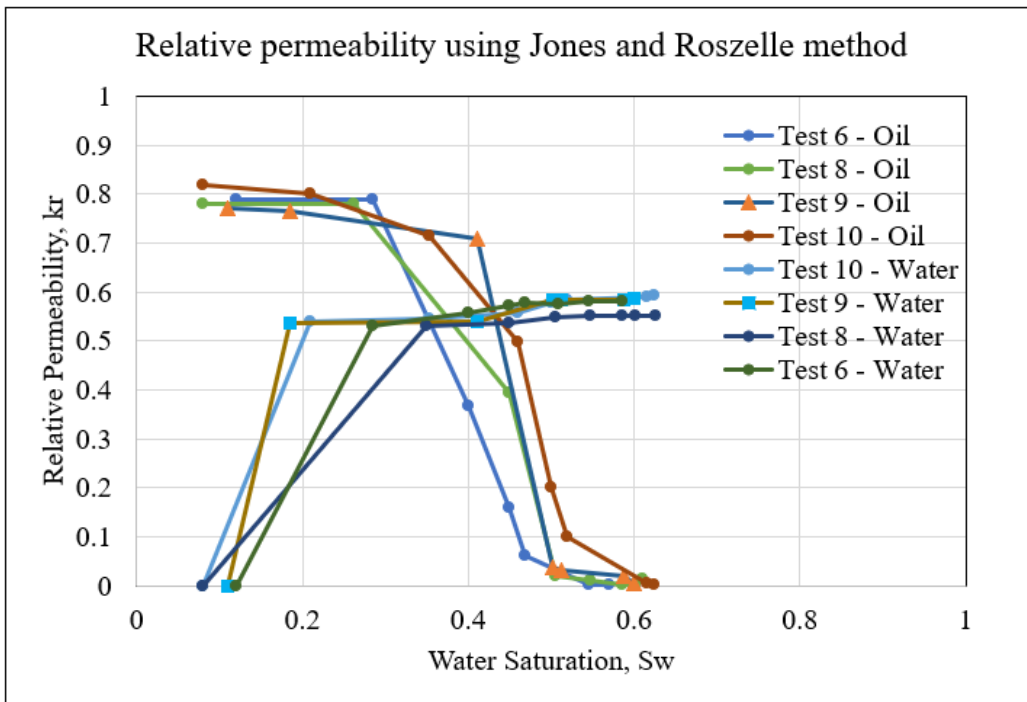


Figure 3.14: Oil and water relative permeability curves at 50° using Jones and Roszelle method.

Oil and water relative permeabilities at 70°C

Figure 3.15 shows the oil and water relative permeability at 70°C by using the DE method. The transition of oil permeability happened very fast between 45% and 60%. Irreducible water saturation was the same as before, around 10%, but residual oil saturation decreased significantly to $S_{or} = 32\%$.

Oil permeability curve obtained by the Jones and Roszelle method was mostly the same as that by the DE method, but between 8% and 55% water saturations was a large gap in the water relative permeability curve because of high injection rate compare with network pore volume. The decrease of residual oil saturation took place as the temperature increased from 20° to 70°C (Figure 3.17), from 49% to 32%. Additional tests were performed at 100°C to validate the conclusion of decrease of oil residual saturation with increasing temperature. Results are shown in Figure 3.17 and 3.18.

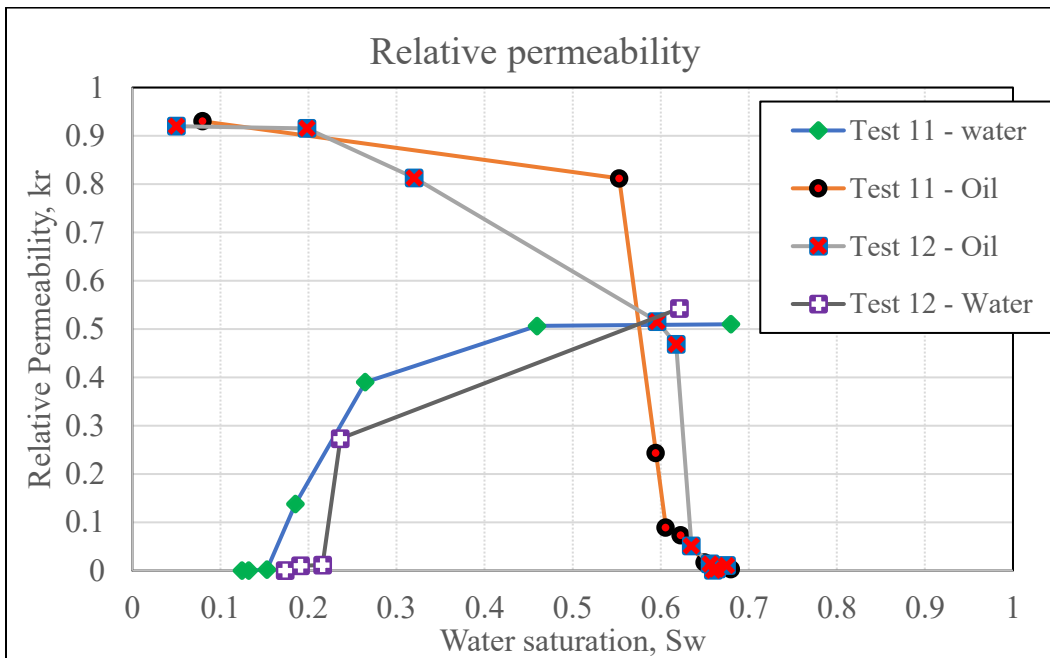


Figure 3.15: Oil and water relative permeabilities at 70° using the DE method.

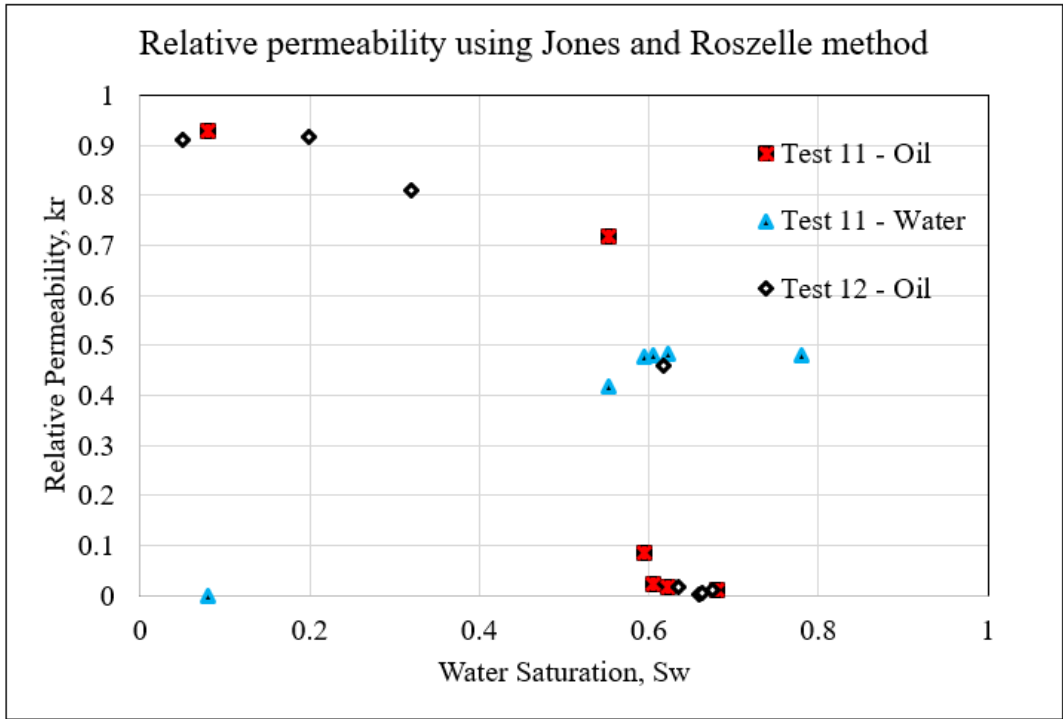


Figure 3.16: Oil and water relative permeabilities at 70°C using the Jones and Roszelle method.

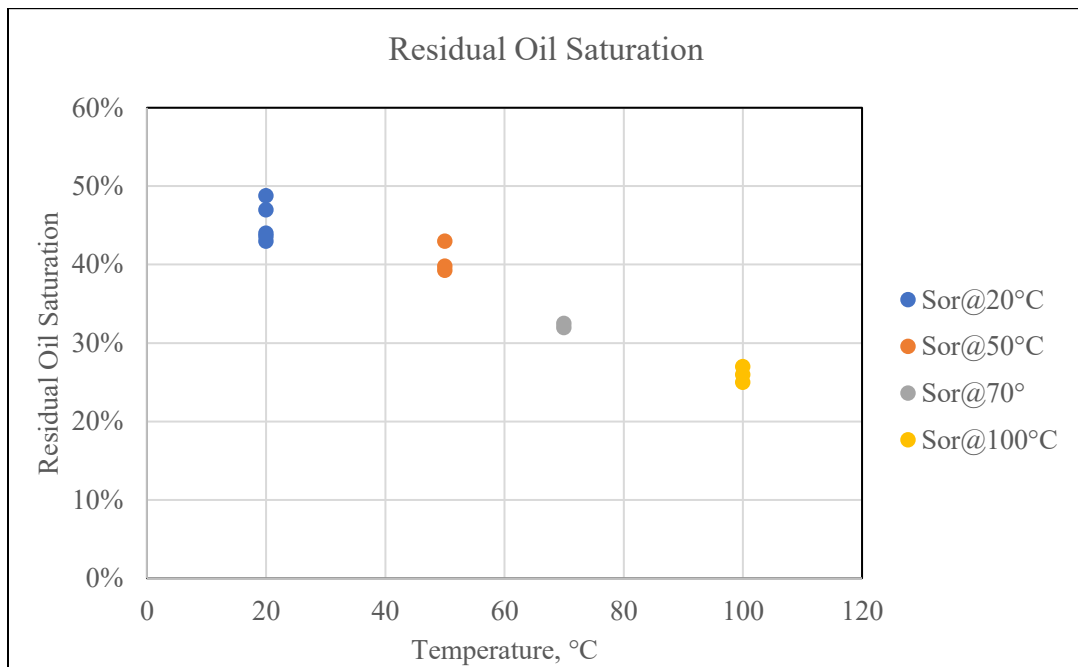


Figure 3.17: Residual oil saturation.

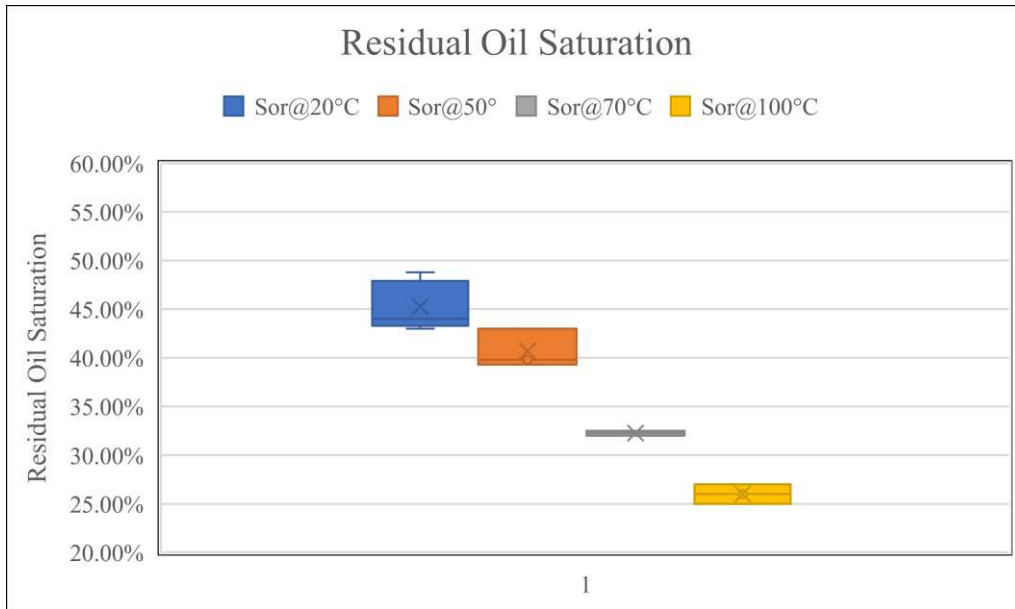


Figure 3.18: Error bars of residual oil saturation change with temperature.

Figure 3.19 compiles oil relative permeability curves from each temperature and water relative permeability curve from one test using DE method.

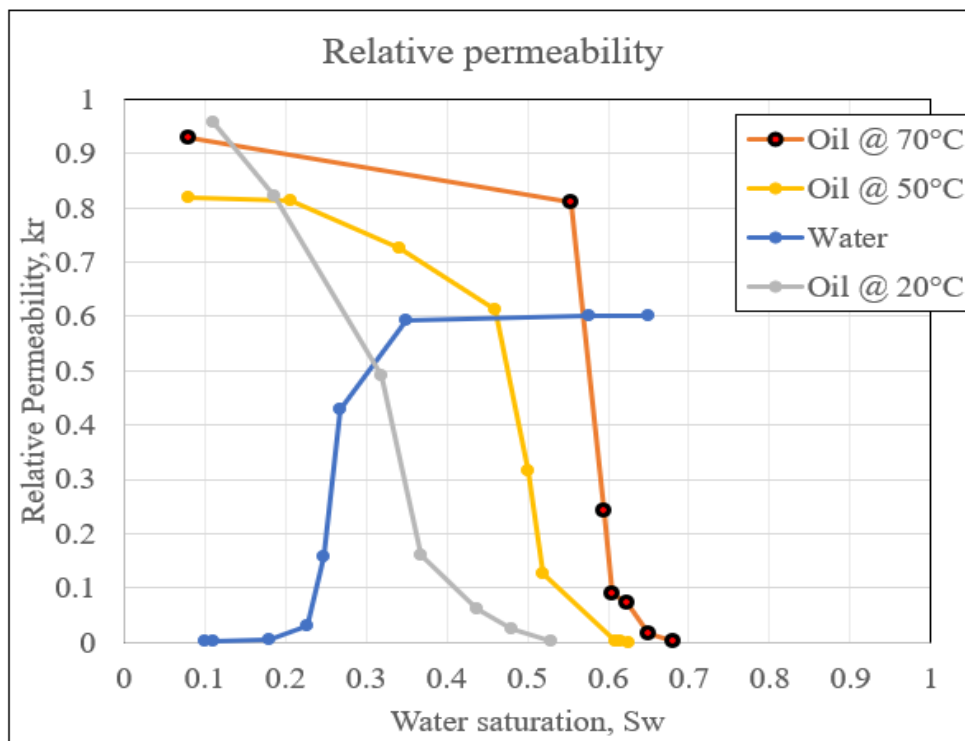


Figure 3.19: Temperature effect on Water – oil permeability curves.

CHAPTER 4

CONCLUSION AND DISCUSSION

In this work we conducted oil and water displacement tests and study the effect of temperature on oil/water relative permeabilities. The two-phase fluid displacement experiments were conducted in microfluidic micromodels, fabricated by soft lithography technique and made by polymer Norland Optical Adhesive 81. It was cured by UV light, which is recommended and proved as most efficient and fast way to precisely bond optical components. Micromodels were perfectly transparent and very stable under pressure.

Two phase flow displacement tests were conducted at constant pressure and all processes were recorded. Captured images were processed and analyzed to obtain porosity of the medium and saturation.

We used the two most common techniques to calculate relative permeabilities under unsteady state condition: the Jones and Roszelle method and the Darcy Equation method. We conducted 12 tests in total to study the effect of temperature on oil and water relative permeability. We observed that residual oil saturation decreased while water irreducible saturation remained unchanged with increasing temperature. The oil relative permeability increased, and water relative permeability curve did not change with temperature and water – oil saturation crossing moved to the high water saturation as temperature increased (Figure 3.19).

The measurements of water relative permeability by the DE method were more accurate than those by the Jones and Roszelle method. The reason was the high injection rate compared with the pore volume of the system, which was around 16 PV and the camera was not able to capture the quick process of water – oil displacement.

The following list of recommendations are presented to improve the estimation of oil – water relative permeabilities from microfluidic micromodels:

1. Use a camera with high fps parameter, that will capture as many images as possible within a second;
2. Conduct an oil – water displacement test and analyze displaced fluid relative permeability (water in this case) using the Jones and Roszelle method;
3. Improve pressure and injection rate measurement for the Jones and Roszelle method.

It also must be noted that the current set-up and approach will not be applicable for gas relative permeability estimations, because gas is more mobile than liquid. Consequently, the gas – oil displacement will proceed much faster than water and oil and capturing detailed images will be very challenging.

Several assumptions have been made in this study, such as ignoring capillary pressure (assuming its negligible compare to the inlet pressure) and no wettability alteration with temperature. Removing these assumptions might lead to more accurate results and more reliable assessment of the effect of temperature on oil/ water relative permeability.

LIST OF SYMBOLS

| | | |
|----------------------|-------|--|
| A | | cross – sectional area, m^2 |
| f | | fractional flow of water or oil, dimensionless |
| $f' = \frac{df}{dS}$ | | fractional flow gradient |
| k | | absolute permeability, m^2 |
| k_e | | effective permeability of oil or water, m^2 |
| k_r | | relative permeability of water or oil, dimensionless |
| $k_{ro,max}$ | | maximum oil relative permeability at the initial water saturation condition (S_{wr}) |
| μ | | dynamic viscosity of water or oil, Pascal * second |
| N_c | | Capillary Number |
| N_p | | volume of oil produced, m^3 |
| NW | | quantity of white pixels in image processing |
| S | | Saturation |
| Q_{wi} | | pore volume injected relative to entire system |
| PV | | pore volume, m^3 |
| p | | pressure, Pascal |
| Δ | | denotes a difference between two quantities |
| x | | fraction of the total length of a system |

u average velocity, m/s

v_s superficial velocity, m/s

L total length of the porous medium, m

λ^{-1} effective viscosity or reciprocal relative mobility

$(u/\Delta p)$ intake capacity at any given displacement or flood stage

$(u/\Delta p)_i$ intake capacity at the very initiation of the flood (S_{wr})

I_r relative injectivity

q volumetric flow rate, m³/s

σ Interfacial tension, mN/m

Subscripts

b refers to single – phase flow or fluid in system on which the absolute permeability is based

d refers to displaced fluid

o oil

w water

x refers to an interior location in a system

2 refers to outlet end location

REFERENCES

- Akhlaghinia, M., Torabi, F., Chan, C. 2013. Estimation of Three-Phase Relative Permeability Isoperms in Heavy Oil/Water/Carbon Dioxide and Heavy Oil/Water/Methane Systems. Presented at the SPE Heavy Oil Conference-Canada, Calgary, Alberta, Canada, June 2013. SPE-165446-MS. <https://doi.org/10.2118/165446-MS>.
- Akin, S., Louis, M., Brigham, W. E. 1999. Effect of Temperature on Heavy Oil/Water Relative Permeabilities. Presented at the International Thermal Operations/Heavy Oil Symposium, Bakersfield, California, March 17–19, 1999. SPE-54120-MS. <https://doi.org/10.2118/54120-MS>.
- Bryant, S. and Blunt, M. 1992. Prediction of relative permeability in simple porous media. *Physical Review A* **46**(4): 2004–2011. <https://doi.org/10.1103/PhysRevA.46.2004>.
- Buckley, S. and Leverett, M. 1942. Mechanism of Fluid Displacement in Sands. *SPE Journal* **146** (01): 107 – 116. SPE-942107-G. <https://doi.org/10.2118/942107-G>.
- Chang, L., Chen, H., Shan, H. et al. 2009. Effect of connectivity and wettability on the relative permeability of NAPLs. *Environ Geol* **56**: 1437 – 1447. <https://doi.org/10.1007/s00254-008-1238-8>.
- Closmann, P. J., Waxman, M. H., and Deeds, C. T. 1988. Steady-State Tar/Water Relative Permeabilities in Peace River Cores at Elevated Temperature. *SPE Reservoir Engineering* **3**(01): 76 – 80. SPE-14227-PA. <https://doi.org/10.2118/14227-PA>.
- Dake, L. P. 1983. *Fundamentals of Reservoir Engineering*, 2nd edition. Amsterdam: Elsevier Science.
- Duffy, D., McDonald, J., and Schueller, O. et al. 1998. Rapid Prototyping of Microfluidic Systems in Poly(dimethylsiloxane). *Analytical Chemistry* **70** (23): 4974 – 4984. <https://doi.org/10.1021/ac980656z>.
- Edmondson, T. A. 1965. Effect of Temperature on Waterflooding. *Journal of Canadian Petroleum Technology* **4** (04): 236 – 242. <https://doi.org/10.2118/65-04-09>.
- Ferer, M., Ji, C., Bromhal, G. S. et al. 2004. Crossover from capillary fingering to viscous fingering for immiscible unstable flow: Experiment and modelling. *Phys. Rev. E* **70** (1):016303. <https://doi.org/10.1103/PhysRevE.70.016303>.
- Grate, J. W., Zhang, C., Wietsma, T. W. et al. 2010. A note on the visualization of wetting film structures and a nonwetting immiscible fluid in a pore network micro-model using a solvatochromic dye. *Water Resour. Res.* **46** (11). <https://doi.org/10.1029/2010WR009419>.
- Johnson, E. F., Bossler, D. P., and Naumann, V. O. 1959. Calculation of Relative Permeability from Displacement Experiments. *SPE Journal* **216** (01): 370-372. SPE-1023-G. <https://doi.org/10.2118/1023-G>.
- Jones, S. C. and Roszelle, W. O. 1978. Graphical Techniques for Determining Relative Permeability From Displacement Experiments. *J Pet Technol* **30** (05):807 – 817. SPE-6045-PA. <https://doi.org/10.2118/6045-PA>.

- Karadimitriou, N. K. 2013. *Two-phase flow experimental studies in micromodels*. Ph D thesis. Utrecht Studies in Earth Sciences, Utrecht, Netherlands.
- Kenzhekhanov, S. 2016. *Chemical EOR Process Visualization using NOA81 Micromodels*. MS thesis, Colorado School of Mines, Golden, Colorado.
- Kumar, M. and Inouye, T. A. 1994. Low-Temperature Analogs of High-Temperature Water/Oil Relative Permeabilities. Presented at the SPE Annual Technical Conference and Exhibition, New Orleans, Louisiana, 25-28 September. SPE-28616-MS. <https://doi.org/10.2118/28616-MS>.
- Lake, L.W. 1989. *Enhanced Oil Recovery*. New Jersey, United States: Prentice Hall Inc.
- Lenormand, R., Zarcone, C., and Sarr, A. 1983. Mechanisms of the displacement of one fluid by another in a network of capillary ducts. *Journal of Fluid Mechanics*, **135**: 337-353. <https://doi.org/10.1017/s0022112083003110>.
- Levachee, B., Azione, A., Bourrel, M. et al. 2012. Engineering the Surface Properties of Microfluidic Stickers. *Lab on Chip* **12**(17): 3028-3031. <https://doi.org/10.1039/c2lc40284j>.
- Lin, B. J. 2009. *Optical Lithography*. SPIE Press. Bellingham, WA, 136.
- Maini, B. B. and Batycky, J. P. 1985. Effect of Temperature on Heavy-Oil/Water Relative Permeabilities and Vertically Drilled Core Plugs. *J Pet Technol* **37**(08):1500-1510. SPE-12115-PA. <https://doi.org/10.2118/12115-PA>.
- Maini, B. B. and Okazawa, T. 1987. Effect of Temperature on Heavy Oil-Water Relative Permeability of Sand. *Journal of Canadian Petroleum Technology* **26**(03): 33-41. PETSOC-87-03-03. <https://doi.org/10.2118/87-03-03>.
- Morrow, N. 1976. Capillary Pressure Correlations For Uniformly Wetted Porous Media. *Journal of Canadian Petroleum Technology* **15**(04). PETSOC-76-04-05. <https://doi.org/10.2118/76-04-05>.
- Morrow, N. 1990. Wettability and Its Effect on Oil Recovery. *J Petr Technol* **42**(12): 1476-1484. SPE-21621-PA. <https://doi.org/10.2118/21621-PA>.
- Mungan, N. 1964. Role of Wettability and Interfacial Tension in Water Flooding. *SPE J* **4**(02):115-123. SPE-705-PA. <https://doi.org/10.2118/705-PA>.
- Muqeem, M., Bentsen, R., and Maini, B. 1995. Effect of Temperature on Three-Phase Water-Oil-Gas Relative Permeabilities of Unconsolidated Sands. Presented at the Technical Meeting / Petroleum Conference of The South Saskatchewan Section, Regina, October 1993. PETSOC-SS-93-03. <https://doi.org/10.2118/SS-93-03>.
- Okabe, H. and Blunt, M. J. 2004. Prediction of permeability for porous media reconstructing using multiple-point statistics. *Physical Review E* **70**(6). <https://doi.org/10.1103/PhysRevE.70.066135>.
- Omar., E. G. B. 2016. *Characterization of two phase flow and transport in porous media through image processing; a micro-scale study in context of enhanced oil recovery*. PhD. Thesis, the University of Manchester. United Kingdom.

- Ortiz – Arango, J. D. 2009. *Pore level Investigation of the Effect of Viscous Coupling, Displacement Flow Rates and Porous Medium Topology on Two-Phase Flow Relative Permeabilities*. MS thesis, University of Calgary, Alberta (April 2009).
- Polikar, M., Ali, F. S. M., and Puttagunta, V. R. 1990. High Temperature Relative Permeabilities for Athabasca Oil Sands. *SPE Res. Eng* **5**(01): 25-32. SPE-17424-PA. <https://doi.org/10.2118/17424-PA>.
- Polikar, M., Ferracuti, F., Decastro, V. et al. 1986. Effect of Temperature on Bitumen-Water End Point Relative Permeabilities and Saturations. *Journal of Canadian Petroleum Technology* **25** (05): 44-50. PETSOC-86-05-04. <https://doi.org/10.2118/86-05-04>.
- Poston, S. W., Israel, S., Hossain, A. K. M. S. 1970. The Effect of Temperature on Irreducible Water Saturation and Relative Permeability of Unconsolidated Sands. *SPE J.* **10**(02): 171-180. SPE-1897-PA. <https://doi.org/10.2118/1897-PA>.
- Qin, Y., Wu, Y., Liu, P. 2018. Experimental studies on effects of temperature on oil and water relative permeability in heavy-oil reservoirs. *Scientific Reports* **8**(01). <https://doi.org/10.1038/s41598-018-31044-x>.
- Quake, S. R. 2000. From micro- to nanofabrication with soft materials. *Science* **290** (5496):1536–1540. <https://doi.org/10.1126/science.290.5496.1536>.
- Ren, L. 2004. *Transport Phenomena in Microfluidic Devices*. PhD. Thesis, University of Toronto, Canada.
- Rogers, J. A. and Nuzzo, R. G. 2005. Recent progress in soft lithography. *Materials today* **8**(2): 50–56. [https://doi.org/10.1016/S1369-7021\(05\)00702-9](https://doi.org/10.1016/S1369-7021(05)00702-9).
- Silvestrini, S., Ferraro, D., Tóth, T. 2012. Tailoring the Wetting Properties of Thiolene Microfluidic Materials. *Lab on a Chip* **12**(20): 4041-4043. <https://doi.org/10.1039/C2LC40651A>.
- Siyang, X., 2016. *Visualization of Crude Oil Displacement by Foam Enhance Oil Recovery (EOR) in Microfluidic Devices*. MS thesis. Rice University, Texas.
- Tsakiroglou, C. D., Theodopoulou, M. A., Karoutsos, V. 2003. Nonequilibrium capillary pressure and relative permeability curves of porous media. *American Institute of Chemical Engineers Journal* **49**(10): 2472-2486. <https://doi.org/10.1002/aic.690491004>.
- Valvatne, P. H. and Blunt, M. J. 2004. Predictive pore-scale modeling of two-phase flow in porous media, using decomposition into prototype flows. *Advances in Water Resources* **24** (3-4): 385-407. <https://doi.org/10.1029/2003wr002627>.
- Wagli, P., Homsy, A. and de Rooij, N. F. 2011. Norland Optical Adhesive (NOA81) Microchannels with Adjustable Wetting Behavior and High Resistance Against a Range of Mid-Infrared-Transparent Organic Solvents. *Sensors and Actuators B Chemical* **156** (2): 994 – 1001. <https://doi.org/10.1016/j.snb.2011.02.005>.
- Wang, W., Shor, L. M., LeBoeuf, E. J. et al. 2005. Mobility of protozoa through narrow channels. *Applied and Environmental Microbiology* **71**(8): 4628-4637. <https://doi.org/10.1128/AEM.71.8.4628-4637.2005>.

- Watson, R. W. and Ertekin, T. 1988. The Effect of Steep Temperature Gradient on Relative Permeability Measurements. Presented at the SPE Rocky Mountain Regional Meeting, Casper, Wyoming, May 11-13. SPE-17505-MS. <https://doi.org/10.2118/17505-MS>.
- Welge, H. J. 1952. A Simplified Method for Computing Oil Recovery by Gas or Water Drive. *Journal of Petroleum Technology* **4**(04): 91-98. SPE-124-G. <https://doi.org/10.2118/124-G>.
- Wu, M., Xiao F., Johnson-Paben, R. M. et al. 2012. Single- and Two-Phase flow in Microfluidic Porous Media Analogs Based on Voronoi Tessellation. *Lab on Chip* **12**(2): 253-261. <https://doi:10.1039/c1lc20838a>.
- Wu, Q., Bai, B., Ma, Y. et al. 2014. Optic Imaging of Two-Phase-Flow Behavior in 1D Nanoscale Channels. *SPE Journal* **19**(05): 793 - 802. SPE-164549-PA. <https://doi:10.2118/164549-PA>.
- Xu, W., Ok, J. T., Xiao, F. et al. 2014. Effect of pore geometry and interfacial tension on water-oil displacement efficiency in oil-wet microfluidic porous media analogs. *Physics of Fluids* **26** (9): 093102. <https://doi.org/10.1063/1.4894071>.
- Yun, W., Ross, C., Roman, S. et al. 2017. Creation of a dual-porosity and dual-depth micromodel for the study of multiphase flow in complex porous media. *Lab on a Chip* **17**(8):1462-1474. <https://doi.org/10.1039/C6LC01343K>.
- Zhang, C., Oostrom, M., Wietsma, T. W. 2011. Influence of Viscous and Capillary Forces on Immiscible Fluid Displacement: Pore-Scale Experimental Study in a Water-Wet Micro-model Demonstrating Viscous and Capillary Fingering. *Energy and Fuels* **25**(8): 3493-3505. <https://doi:10.1021/ef101732k>.
- Zhang, L., Tong, J., Xiong, Y. 2017. Effect of temperature on the oil–water relative permeability for sandstone reservoirs. *International Journal of Heat and Mass Transfer* **105**: 535 – 548. <https://doi.org/10.1016/j.ijheatmasstransfer.2016.10.029>.

APPENDIX A

From Darcy's law, for the two phases, oil and water,

$$q_o = -\frac{k_o A}{\mu_o} \left(\frac{\partial P_o}{\partial x} \right) \quad (\text{A.1})$$

$$q_w = -\frac{k_w A}{\mu_w} \left(\frac{\partial P_w}{\partial x} \right) \quad (\text{A.2})$$

If we assume water to be the wetting phase in the system, the capillary pressure is:

$$P_c = P_o - P_w \quad (\text{A.3})$$

Continuity equation to each phase which is assumed incompressible:

$$\frac{\partial q_o}{\partial x} = -\phi A \frac{\partial S_o}{\partial t} \quad (\text{A.4})$$

$$\frac{\partial q_w}{\partial x} = -\phi A \frac{\partial S_w}{\partial t} \quad (\text{A.5})$$

Also, the sum of the saturations is equal to 1, thus:

$$S_w + S_o = 1.0 \quad (\text{A.6})$$

The combination of Equations 6.4 through 5.6 gives

$$\frac{\partial}{\partial x} (q_o + q_w) = 0 \quad (\text{A.7})$$

which means the total flow rate $q_t = q_o + q_w$ is constant. Combining Equations 5.1 through 5.3 to eliminate P_o and P_w ,

$$q_o = -\frac{k_o A}{\mu_o} \left[-\frac{q_w \mu_w}{k_w A} + \frac{\partial P_c}{\partial x} \right] \quad (\text{A.8})$$

Fractional flow, f_w , from flowing stream,

$$f_w = \frac{q_w}{q_o + q_w} \quad (\text{A.9})$$

By neglecting the effect of capillary pressure gradient in Equation 5.7,

$$q_o = \frac{k_o A}{\mu_o} \left[\frac{q_w \mu_w}{k_w A} \right] \quad (\text{A.10})$$

and substituting q_o from Equation 5.10 in Equation 5.9,

$$f_w = \frac{q_w}{\left(\frac{k_o A}{\mu_o} \right) \left[\frac{q_w \mu_w}{k_w A} \right] + q_w} \quad (\text{A.11})$$

or

$$f_w = \frac{1}{1 + \left[\frac{f_o \mu_w}{k_w \mu_o} \right]} \quad (\text{A.12})$$

APPENDIX B

Here, we present the MATLAB code, example of image segmentation and conversion of pixels ratio to phase saturation

1. Image segmentation

```
function [BW,maskedImage] = segmentImage(RGB)
```

```
%segmentImage Segment image using auto-generated code from imageSegmenter app
```

```
% [BW,MASKEDIMAGE] = segmentImage(RGB) segments image RGB using
```

```
% auto-generated code from the imageSegmenter app. The final segmentation
```

```
% is returned in BW, and a masked image is returned in MASKEDIMAGE.
```

```
% Auto-generated by imageSegmenter app on 08-Nov-2020
```

```
%-----
```

```
% Convert RGB image into L*a*b* color space.
```

```
X = rgb2lab(RGB);
```

% Graph cut

foregroundInd = [1796295 1983056 2250300 2310872 2310877 2316888 2973719 3284910
3656455 3880845 4188597 5161379 5161382 5165572 5171422 5177446];

backgroundInd = [67557 67560 73543 73554 73565 73573 73581 73584 77499 77513 77524
77537 77548 83493 83496 83510 89493 89506 95481 95495 95500 99484 105494 111504 117515
121514 127525 133500 133513 133524 133535 133538 137235 137243 137249 137257 137265
137273 137279 137287 137290 137295 137301 137306 137311 137320 137325 137344 137358
137374 137393 137410 137426 137431 137448 137469 137486 137499 137502 143169 143213
143216 143240 149109 2605242 2617262 2639386 2639391 2643440 2643443 2649379 2649448
2655354 2655624 2659626 2665675 2671486 2671661 2681529 2693664 2699688 2699819
2703601 2703721 2703775 2703835 2709696 2715725 2719668 2725844 2731871 2737900
2737906 2741908 2741990 2747793 2747929 2753804 2759759 2760037 2760062 2763884
2763950 2764081 2769906 2776020 2779954 2779976 2780017 2780147 2792032 2792059
2792116 2797993 2802012 2817989 2818098 2818117 2818302 2840167 2840363 2852201
2858181 2858309 2862252 2862325 2868322 2868409 2874330 2874453 2878316 2878351
2878354 2890282 2890585 2896426 2896524 2896609 2912564 2918639 2934573 2938589
2944493 2944569 2950620 2960587 2966692 2972716 2972896 2982656 2988682 2988794
2988925 2988936 2994802 2994886 2994949 2998889 3004738 3004850 3010825 3010915
3026859 3026916 3026973 3027071 3027099 3032918 3033060 3037013 3037152 3037155
3043037 3048914 3058973 3064995 3065242 3071133 3071266 3077198 3077290 3077331
3081230 3087088 3087251 3087311 3093354 3097142 3097144 3097163 3097166 3097191
3097193 3097204 3103313 3109421 3125210 3125349 3125373 3125485 3131242 3131422
3131452 3131506 3131542 3137263 3137446 3141424 3163354 3163506 3163553 3163596

3163624 3169383 3169577 3175563 3179589 3179603 3179633 3179658 3185567 3185682
3191463 3191722 3195509 3195512 3195553 3201743 3201806 3201814 3201816 3207549
3207584 3207751 3207808 3213796 3213802 3213821 3213840 3217553 3217690 3217761
3217807 3223575 3223624 3223665 3223667 3223825 3229634 3229645 3229806 3235748
3235830 3235952 3239731 3245723 3245747 3251706 3255831 3261716 3261964 3273884
3277804 3277897 3278101 3283828 3289820 3289822 3289953 3289956 3290021 3290095
3290122 3299846 3305867 3306085 3306126 3306129 3311886 3311932 3311949 3315951
3316093 3328075 3328184 3334056 3334072 3334075 3334094 3334126 3337971 3344221
3356043 3356046 3356048 3356171 3360072 3360157 3360160 3360250 3366110 3366126
3366143 3366145 3366162 3366165 3372254 3376281 3376284 5006927 5029034 5044858
5045120 5050882 5056906 5066943 5067232 5072967 5073275 5079316 5079326 5079340
5083007 5083375 5095053 5101077 5101799 5105793 5105796 5105801 5105806 5105812
5110991 5111114 5111798 5117803 5127061 5127175 5127818 5139220 5139223 5139836
5139839 5143127 5149258 5155873 5155876 5165221 5165313 5165316 5165679 5171335
5177356 5183296 5183377 5183751 5183958 5187391 5193338 5193406 5193409 5193412
5193979 5199365 5199398 5199400 5199411 5199417 5199422 5199425 5203381 5203831
5203986 5209405 5231943 5241737 5241756 5241767 5241778 5241781 5241789 5241795
5248009 5254041 5254044 5254061 5254080 5254096 5254104 5254107 5254110];

```
L = superpixels(X,26405,'IsInputLab',true);
```

```
% Convert L*a*b* range to [0 1]
```

```
scaledX = prepLab(X);
```

```
BW = lazysnapping(scaledX,L,foregroundInd,backgroundInd);
```

```
% Create masked image.
```

```
maskedImage = RGB;
```

```
maskedImage(repmat(~BW,[1 1 3])) = 0;
```

```
end
```

```
function out = prepLab(in)
```

```
% Convert L*a*b* image to range [0,1]
```

```
out = in;
```

```
out(:,:,1) = in(:,:,1) / 100; % L range is [0 100].
```

```
out(:,:,2:3) = (in(:,:,2:3) + 100) / 200; % a* and b* range is [-100,100].
```

```
end
```

2. Phase saturation

```
clear;
```

```

clear all;

W = imread('WO2.jpg');

imshow(W)

W1 = segmentImage(W);

imshow(W1);

%% Calculate B&W area

W2 = im2double(W1);

k = regionprops(W2);

% Find black pixels

b = find(W2==0);

% Find white pixels

w = find(W2==1);

numBpixels = numel(b);

numWpixels = numel(w);

%%Calculate minimum area which represents empty network

Roc_Oil_area = numBpixels*100/(numWpixels+numBpixels);

Water_area = numWpixels*100/(numWpixels+numBpixels);

```